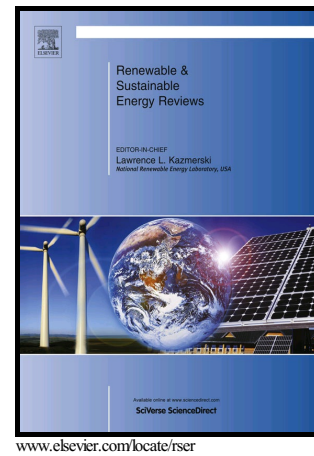# Author's Accepted Manuscript

Diffuse solar irradiance estimation on building's façades: review, classification and benchmarking of 30 models under all sky conditions

Miguel de Simón-Martín, Cristina Alonso-Tristán, Montserrat Díez-Mediavilla

Cite this article as: Miguel de Simón-Martín, Cristina Alonso-Tristán and Montserrat Díez-Mediavilla, Diffuse solar irradiance estimation on building' façades: review, classification and benchmarking of 30 models under all sky c o n d i t i o n s , *Renewable and Sustainable Energy Reviews* http://dx.doi.org/10.1016/j.rser.2017.04.034

# Diffuse solar irradiance estimation on building's façades: review, classification and benchmarking of 30 models under all sky conditions

Miguel de Simón-Martín[a,b,*], Cristina Alonso-Tristán[b], Montserrat Díez-Mediavilla[b]

[a]*Energy Resources' Smart Management (ERESMA) Research Group, University of León.*
*Escuela Superior y Técnica de Ingenieros de Minas, Campus de Vegazana s/n, 24071, León (Spain).*
[b]*Solar and Wind Feasibility Technologies (SWIFT) Research Group, University of Burgos.*
*Escuela Politécnica Superior, Campus de Río Vena s/n, 09006, Burgos (Spain).*

## Abstract

Solar energy potential analysis on oriented and tilted surfaces, such as building façades, is of capital importance to estimate the energy production potential in integrated systems, such as BIPVs. The spatial distribution of solar diffuse energy outstands as one of the most critical factors in order to improve performance simulations. Nevertheless, most wide spread models have been only evaluated on equator facing tilted surfaces and with daily mean or hourly mean time ranges. Thus, in this paper, 30 transposition solar diffuse irradiance models, from the semiphysical classical ones to the newest non-parametric models, are reviewed, classified according to their characteristics and evaluated against empirical 10-min averaged diffuse irradiance values gathered from high precision pyranometers placed on vertical positions facing the four cardinal directions. Models' performance is evaluated by several statistical estimators and a benchmark has been carried out by a non-parametrical aggregating procedure. Results show that the most accurate models appear to be the non-parametric ones. From these, The Multi-Layer Perceptron obtains the best results. From the parametric models, the one whose estimations are closest to the measures is the Perez et al. with local optimised coefficients. Perez et al. model with the original coefficients, Skartveit & Olseth and Igawa et al. models also show a good performance.

*Keywords:* diffuse solar irradiance, vertical surfaces, irradiance modelling, sky conditions, benchmarking.

## 1. Introduction

It is clear that gaining an in-depth knowledge of the available solar resource is of the utmost importance. It can be used in very different fields, such as meteorological forecasting, biology, agriculture, energy, architecture, and so on. Moreover, it should not be forgotten that knowledge of the potential of solar radiation is necessary for diversifying energy and dimensioning heating and air-conditioning systems, as well as for the intelligent use of renewable energies on most scenarios. The design, dimensioning and calculation of solar-energy-based systems requires precise knowledge of the amount of global irradiance and specially the direct, diffuse and reflected components that fall on surfaces that are horizontal or inclined in any direction. This late case is really worth of interest on the analysis of building's efficiency or solar energy generators performance. The fruit of studies in this field allows the development and implementation of many different systems; for example photovoltaic technology [1, 2, 3, 4], the calculation of thermal loads and cooling in buildings [5], the design of efficient solar collectors [6], and an infinite number of other technological applications that have the objective of increasing human well-being and comfort [7, 8].

Since the Maastricht Treaty in 1992 [9], the European Union's energy and environmental target has been to promote sustainable and environmentally friendly growth in its member countries. Having set the goal of a 12.5% contribution from renewable energies with respect to total consumption for the year 2010, at the 2004 Berlin Conference [10] the recommendation was made that the percentage of renewable energies for the year 2020 should reach 20% of the total consumption of energy [11]. This was established through the Horizon

---

*Corresponding author at: Department of Electric, Systems and Automatics Engineering. University of León (Spain). Campus de Vegazana s/n, 24071. Tel.: +34 987 29 10 00 5391.

*Email addresses:* `miguel.simon@unileon.es` (Miguel de Simón-Martín), `catristan@ubu.es` (Cristina Alonso-Tristán), `mdmr@ubu.es` (Montserrat Díez-Mediavilla)

**Nomenclature and abbreviations**

| | | | | | | |
|---|---|---|---|---|---|---|
| $A_i$ | Anisotropic index | [-] | $R_r$ | Tilted reflected irradiance fraction | [-] |
| $b$ | Radiance distribution index | [-] | RMSD | Root Mean Squared Difference | [W·m$^{-2}$] |
| $B$ | Beam direct irradiance | [W·m$^{-2}$] | $s_c$ | Circumsolar fraction | [-] |
| $B_{ext}$ | Extraterrestial irradiance | [W·m$^{-2}$] | Si | Igawa's sky index | [-] |
| $B_{sc}$ | Solar constant | [W·m$^{-2}$] | $T_M$ | Muneer's radiance distribution | [-] |
| $d$ | Willmott's index of agreement | [-] | **Greek symbols** | | |
| $D$ | Diffuse irradiance | [W·m$^{-2}$] | $\alpha$ | Significance level | [-] |
| $f_b$ | Shadowing coefficient | [-] | $\gamma$ | Azimuth angle | [rad] |
| $f_c$ | Blocked circumsolar | [-] | $\gamma_p$ | Sensor's azimuth angle | [rad] |
| $G$ | Global irradiance | [W·m$^{-2}$] | $\gamma_s$ | Sun's azimuth angle | [rad] |
| $G_{st}$ | Standard global irradiance | [W·m$^{-2}$] | $\Delta$ | Perez et al.'s brightness index | [-] |
| $h_s$ | Solar elevation | [rad] | $\delta_s$ | Sun's declination angle | [rad] |
| $i_{gr}$ | Rel. ground radiance function | [-] | $\varepsilon$ | Perez et al.'s clearness index | [-] |
| $i_r$ | Rel. sky radiance function | [-] | $\theta_z$ | Zenith angle | [rad] |
| $I$ | Sky radiance | [W·m$^{-2}$·sr$^{-1}$] | $\theta_{zp}$ | Sensor's zenith angle | [rad] |
| $I_g$ | Albedo's radiance | [W·m$^{-2}$·sr$^{-1}$] | $\theta_{zs}$ | Sun's zenith angle | [rad] |
| $I_{gz}$ | Nadith radiance | [W·m$^{-2}$·sr$^{-1}$] | $\mu_{1-\alpha}$ | Estatistical estimator | [W·m$^{-2}$] |
| $I_z$ | Zenith radiance | [W·m$^{-2}$·sr$^{-1}$] | $\xi_{gp}$ | Reflectance angle | [rad] |
| $k_d$ | Diffuse fraction | [-] | $\xi_{op}$ | Obstacle-pyranometer angle | [rad] |
| $m$ | Relative optical air mass | [-] | $\xi_p$ | Sensor-sky point angle | [rad] |
| MBD | Mean Bias Difference | [W·m$^{-2}$] | $\xi_s$ | Sun-sky point angle | [rad] |
| $N$ | Day of the year | [day] | $\xi_{sp}$ | Sun-pyranometer angle | [rad] |
| $R$ | Reflected irradiance | [W·m$^{-2}$] | $\rho$ | Ground's reflectance | [-] |
| $R^2$ | Coefficient of determination | [-] | $\tau$ | Atmosphere's transmitance | [-] |
| $R_b$ | Tilted beam irradiance fraction | [-] | $\phi_g$ | Geographical latitude | [deg. N] |
| $R_d$ | Tilted diffuse irradiance fraction | [-] | | | |

2020 plan [12]. Prescriptions were also made in the Kyoto Protocol on climate change [13], which many European countries, including Spain, signed up to. As it is well known, the protocol created an obligation to lower emissions of greenhouse gases such as $CO_2$, which are produced mainly by the majority of transportation forms and by current systems for generating thermal and electrical energy. Within this framework, one of the paths to the achievement of the stated objectives is the development of new energy strategies within urban environments.

A significant level of energy is consumed in urban environments. Policies focused on distributed generation, net energy balance or the construction of *"Nearly Zero Energy Buildings"* (nZEB) have been supported by both photovoltaic and thermal solar technology through their modularity and easy adaptability to any structure. The nZEB concept has been considerably strengthened by European energy policies such as EU Directive 2002/91/EC [14], consolidated in Directive 2010/31/EU [15], which demands that, since 2019, all newly constructed buildings that are property of public entities

must be nZEBs, and that by the end of 2020 all newly constructed buildings must be of this type. This new construction trend allows buildings to be practically independent from the electricity network and other energy infrastructure, thanks mainly to the integration of sources of renewable energy in the architectural design (particularly in *"Building Integrated Photovolatic Systems"* or BIPVs), maximization of ventilation and natural light, a lowering and optimization of consumption, and so on [16, 17].

The integration of photovoltaic generators in buildings envelopes, giving rise to BIPV systems, offers immense potential. In Germany, for example, the integration of photovoltaic systems in buildings may allow up to 50% of demand for electricity to be covered [18]. Other studies indicate that there could be electrical energy savings of between 30% and 50% [19]. In any case, there would be a significant advance towards energy sustainability and self-sufficiency and, therefore, this development seems like it will be unstoppable in the coming years. Furthermore, the harnessing of solar energy via building façades can be achieved in many
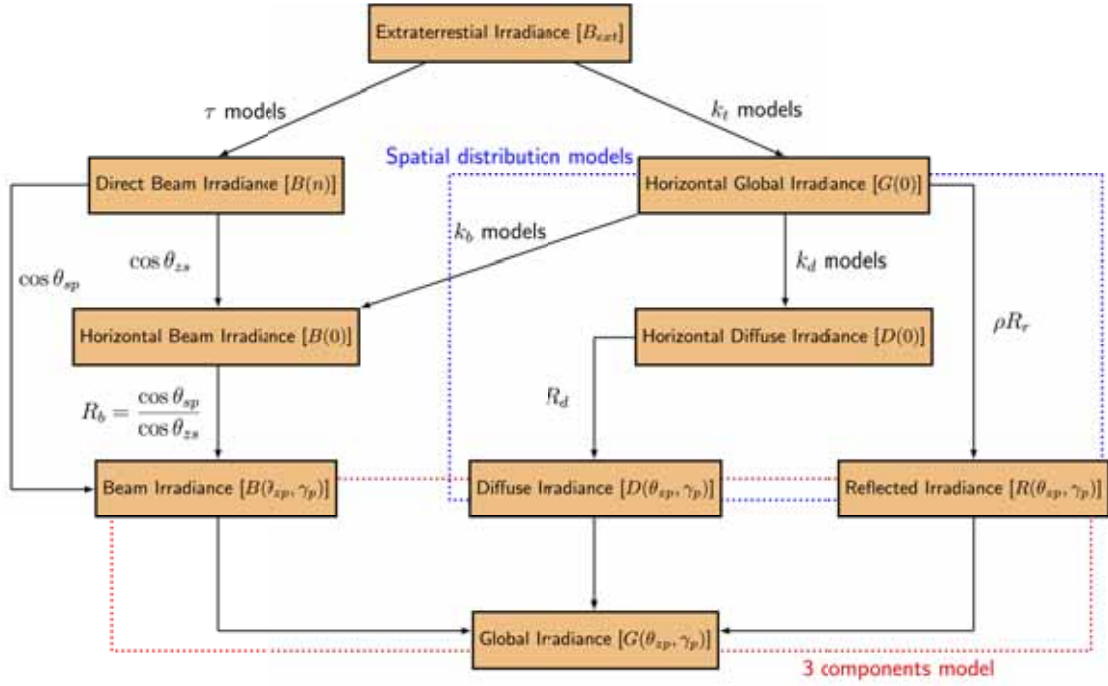
Figure 1: Solar irradiance modelling flow chart.

ways, and especially through the incorporation of thermal and photovoltaic modules [20].

Paradoxically, the development of solar energy systems in recent decades, while extensive, has always been focused on large energy-production plants (popularly known as solar farms) or, in contrast, on small and isolated facilities in rural settings that need an autonomous energy supply. According to [21], grid-connected decentralized PV power plants have decreased from more than the 80% in 2000 to almost the 30% in 2015. Moreover, although the rapid deployment of grid-connected PV dwarfed the off-grid market, off-grid applications are developing more rapidly in several countries than in the past and some targeted support has been implemented [21]. Both scenarios differ completely from the average situation of an urban environment [22, 23, 24]. Beam direct irradiance on any surface depends on the cosine of the incidence angle which can be evaluated through the description of the Sun's position in the sky vault. However, spatial distribution of the diffuse irradiance is affected by the atmosphere conditions and the observed part of the sky vault by the studied surface. A deep analysis need to be conducted in order to develop effective tools that allow the use of the solar resource and an optimal design of urban solar plants.

Characterising solar energy is a complex task. The irradiance from the sun that reaches the outer part of the atmosphere can be considered as practically constant over time for the purpose of this analysis (hence the definition of the solar constant as irradiance at the extraterrestrial level, with a value of $B_{sc} = 1\,367$ W·m$^{-2}$ [25]). However, the irradiance that reaches any point on the Earth's surface is affected by quasi-random phenomena such as the absorption and scattering produced by the gases of the atmosphere, aerosols or particles in suspension. For this reason, obtaining systematic and reliable measures of solar potential at the surface level is fundamentally important and not a trivial matter [26]. Also, despite the increase over the last decade in climatological stations with the capacity to measure variables related to the magnitudes of solar irradiance in developed countries, the density of these stations is still very low due to the extent of the Earth's surface. To give an example, on average, ground stations in the United States in 2008 covered approximately 1% of the territory. The world average is estimated at 5% [27]. Moreover, databases that recorded ground measures are not always complete, especially with regard to the measuring of the components of irradiance, due to cost and the difficulties of calibrating, operating and maintaining of the equipment. This leads directly to the need to develop

3

and validate models or theories that allow us to estimate irradiance values from the available set of data, in the simplest and most precise way possible.

As it can be seen in Figure 1, modelling diffuse irradiance on tilted (including vertical) surfaces requires several transformations and chains of models depending on the available model input data. Direct beam irradiance $B(n)$ can be estimated from the extraterrestrial irradiance value $B_{ext}(n)$, through the $\tau$ models which calculate the atmosphere's transmittance values on the horizontal surface. On the other hand, $k_t$ models correlate the extraterrestial irradiance with the horizontal global irradiance and $k_d$ and $k_b$ models allow the evaluation of the diffuse and beam fractions respectively. Reflected irradiance on a given surface, $R(\theta_{zp}, \gamma_p)$, is proportional to the albedo's reflectance $\rho$ and the horizontal global irradiance. The so-called *"transposition models"* transform global horizontal and diffuse horizontal irradiances into reflected and diffuse irradiances on any given plane ($R_d$ and $R_r$ values) tilted a zenith angle $\theta_{zp}$ and oriented an azimuth angle $\gamma_p$. Moreover, most of the models found in the literature have been developed and tested with irradiance data on inclined planes pointing the Equator (equatorial direction) and not a convention on the nomenclature has been achieved.

Although it can be found a wide range of models for the transposition of the irradiance value from the horizontal plane to Equator pointing tilted surfaces, not an extended systematic review and validation test on several vertical planes has been found in the consulted bibliography. Furthermore, most of previous works in this field limit the analysis to whether clear sky conditions or complete overcast skies and use indirect data from the composition model instead of direct measurements of diffuse irradiance on the tilted plane. Moreover, a classification of the transposition models according to their adopted hypothesis and formulation has been found worth of interest and it helped the authors in this work to propose a normalized nomenclature for all models. Thus, a deep and systematic review of these models has been carried out and a benchmarking analysis has been conducted with measurements on four oriented vertical surfaces under all sky conditions.

## 2. Materials and Methods

Data used in the study were acquired at a radiometric station installed on the rooftop of the E.P.S. of the University of Burgos (42.2122°N, 3.3753°W, 860 m.a.s.l.). Obstacles on the horizon are negligible (elevation angles are less than 5°) and top quality standards according to the World Meteorological Organi-

zation (WMO) [28] and the National Renewable Energy Laboratory from United States (NREL) [27] are guaranteed. The data set included diffuse irradiance measures, taken every ten minutes on vertical planes oriented toward the four main cardinal points (North, South, East and West) by the MK6 device, which has four sensors (First class pyranometers) and one single multi-lobular shadow-band. This device has been presented and fully described in [29]. The study period encompassed eight months, from September 2014 to April 2015, so as to ensure that a variety of seasonal processes and meteorological conditions were sampled. Other studies in the bibliography use typically periods for measurement from 3 months to one year hourly or 10-min data [30, 31, 32, 33, 34]. Moreover, due to the novelty of the deployed measurement instrument for the vertical diffuse irradiance, it is not possible to access to a wider range of data.

Geometrical correction and Le Baron total correction have been applied to the measures to reduce the influence of the shadow-band and obtain high accuracy values [35, 36]. Albedo's irradiance have been quantified by a SIR SKS-1110 pyranometer installed in an inverted position.

Horizontal measures of global and diffuse irradiance have also been obtained with Hukseflux SR11 pyranometers mounted on a Geonica SunTracker-3000. Correction factor for the diffuse irradiance measurement in this case is almost negigible as the sun tracker has a ball that prevents the direct beam irradiance from reaching the diffuse sensor. Direct beam irradiance has been measured with a Hukseflux DR01 pyrheliometer.

The following quality physical filters, proposed in [28, 37, 38, 39], were applied to guarantee reliable data:

1. Solar elevation $h_s \geq 5°$.
2. $G(0) \geq 0.19$ W·m$^{-2}$.
3. $G(0) \leq 1.12 B_{sc}$.
4. $B(n) \leq B_{sc}$.
5. $B(n) \geq 0.19$ W·m$^{-2}$.
6. $B(n)/B_{sc} \leq G(0)/(B_{sc} \cos \theta_{zs}) - 0.5$.
7. $D(0) \leq 1.15 G(0)$.
8. $D(0) \leq 0.8 B_{sc}$.
9. $D(0) \geq 0.19$ W·m$^{-2}$.
10. $R(180) \geq 0.19$ W·m$^{-2}$.
11. $R(180) \leq G(0)$.

All pyranometers were calibrated against a reference pyranometer (Hukseflux SR21) which had in turn been previously calibrated at the World Radiation Center (WRC) in Davos (Switzerland). The uncertainties of all the sensors were calculated by the B method proposed in [40] and the results are shown in Table 1.

Table 1: Sensor's uncertainties.

| Measure | Sensor | Max. Relative Uncert. [%] |
|---------|--------|---------------------------|
| Diff. North | Hukseflux SR11 | 5.6 |
| Diff. South | Hukseflux SR11 | 5.6 |
| Diff. East | Hukseflux SR11 | 5.6 |
| Diff. West | Hukseflux SR11 | 5.6 |
| Glo. Hor. | Hukseflux SR11 | 4.2 |
| Diff. Hor. | Hukseflux SR11 | 4.6 |
| Dir. Beam | Hukseflux DR01 | 5.5 |
| Albedo's | SIR SKS-1110 | 7.8 |

Non-parametric models have been evaluated through a $k$ cross-validation method. Thus, for these models, the whole data set was randomly divided into $k = 10$ subsets of an approximately equal size. Throughout the $k = 10$ iterations, one subset was the test data set and the combination of the other nine subsets was the training subset. The training subsets were used to adjust the coefficients of the models and the test subset was used to evaluate the performance of the model. The whole procedure was repeated in such a way that every subset is used once for testing. Note that the testing data for each subset was not used in the training of the model. Model performance was finally established as the average value over the $k = 10$ iterations obtained by the statistical estimators that were adopted.

Six parameters were considered for the statistical analysis: coefficient of determination ($R^2$), the Root Mean Squared Difference (RMSD), the Mean Bias Difference (MBD), $t$-statistic ($t$), Willmott's index of agreement ($d$) and the $\mu_{1-\alpha}$-statistic ($\mu_{0.99}$). Their expressions are defined by equations (1), (2), (3), (4), (5) and (6), respectively [41].

$$R^2 = \frac{\sigma_{XY}^2}{\sigma_X^2 \sigma_Y^2}, \qquad (1)$$

$$\text{RMSD} = \sqrt{\frac{1}{N}\sum_{i=1}^{N}(D_{e,i} - D_{m,i})}, \qquad (2)$$

$$\text{MBD} = \frac{1}{N}\sum_{i=1}^{N}(D_{e,i} - D_{m,i}), \qquad (3)$$

$$t = \sqrt{\frac{(N-1)\text{MBD}^2}{\text{RMSD}^2 - \text{MBD}^2}}, \qquad (4)$$

$$d = 1 - \frac{\sum_{i=1}^{N}(D_{e,i} - D_{m,i})^2}{\sum_{i=1}^{N}(|D_{e,i} - \overline{D}_m| + |D_{m,i} - \overline{D}_m|)^2}, \qquad (5)$$

$$\mu_{1-\alpha} = \text{sign(MBD)}\left(|\text{MBD}| - t_{\alpha/2}\sqrt{\frac{\text{RMSD}^2 - \text{MBD}^2}{N-1}}\right), \qquad (6)$$

where, $\sigma_{XY}$ is the covariance between the $X$ (measured values) and the $Y$ (estimated values) variables, $\sigma_X$ is the standard deviation of variable $X$, $\sigma_Y$ is the standard deviation of variable $Y$, $D_{e,i}$ is the $i$-th diffuse estimated value, $D_{m,i}$ is the $i$-th diffuse measured value, $\alpha$ is the statistical significance (usually taken 0.01) and $N$ is the total number of measures.

The RMSD value points to the short-term behavior of the model, while the MBD value describes its long-term performance. We should highlight that a few differences of a high magnitude with regard to the reference values will significantly increase the RMSD. Conversely, overestimations can be canceled out by under-estimations in the MBD. Moreover, neither the RMSD nor the MBD can provide a confidence interval to give significance to the model's predictions. Thus, in equation (4) the $t$-statistic is presented [42]. It combines both statistical estimators and offers a confidence interval with a statistical significance of $\alpha$. However, this estimator is based on a very restrictive hypothesis contrast where the mean difference between the estimated and the reference values is assumed to be zero ($\mu = 0$). This estimator was redefined in terms of the value of such a difference, in order to avoid such a limiting restriction, and is now called $\mu_{1-\alpha}$ [35]. In this case, we took $\alpha = 0.01$. This estimator includes the sign of the MBD value, in order to analyze whether the proposed model tended either to overestimate (positive sign) or underestimate (negative sign). Finally, Willmott's $d$ estimator [43] represents the relative distance among the measured values and the estimated values against the centered distance (without systematic error). Its value is ranged in the interval $d \in [0, 1]$.

For the final decision, 5 rankings (one for each particular direction and one for the overall behavior) including the 30 models under study were included. The overall or final rankings were calculated by a non-parametric aggregation procedure, adapted from [44]. In this case, the locations were substituted by the measured directions.

In all cases, studentized residuals [45] were evaluated and absolute values greater than 2 were discarded.

Thus, normality, homocedasticity and the independence of the data were found to be acceptable.

In the case of radiance gradient anisotropic models, certain complex integrals must be carried out through the zenith and the azimuth angles. In this work, numerical integration methods using global adaptive quadrature and default error tolerances implemented in Matlab routines have been used.

Finally, Taylor diagrams [46] for the four cardinal directions are plotted as part of a graphic analysis, and Pairwise matrix rankings of the overall performance have been obtained for MBD, RMSD and $\mu_{0.99}$ statistical estimators.

## 3. Models classification and description

According to [47], a literature review can be conducted in many different ways. In order to show the state of the art in this field with precision, it has been decided to conduct a systematic review. In [48] a systematic review is defined as a process developed to identify the core of a narrative review which may result worth of interest in practice. This process is carried out by following a scientific, well-documented and objective procedure which takes 6 steps:

1. Identify the review purpose and formulate the research question.
2. Define the literature searching criteria.
3. Conduct the literature review.
4. Evaluate the data.
5. Anaylse and synthesize the data.
6. Show the results and conclusions.

Then, following the described process, we have defined the aim of the study and the research question as *"which models can be used to estimate the diffuse irradiance component on tilted and oriented surfaces?"* The proposed question fulfills the requirements exposed in [49]: the question is delimited and it is accesible and distinguishable in the literature.

According to the systematic review procedure, next step requires the definition of the details of the searching criteria. In this case it has been considered the following:

**Sources:** Only papers from indexed international journals, scientific books edited by international editors, international conference proceedings, open access Ph.D. Thesis and technical reports from prestigious international organizations have been included in the research.

**Language:** English and Spanish.

**Publication period:** As it is desired to include the original models' definitions in order to avoid errata from replication in other contributions, it has been analysed research works from 1940 until 2016.

**Requirements:** Selected contributions must be open access or available in international databases, peer-reviewed and guarantee traceability in the research. From those contributions which were presented both for a journal paper and a conference communication, only the journal manuscript will be included in the review.

**Type:** Both original research contributions (new model descriptions) and review works have been included in the analysis.

Once the searching criteria were defined, the literature review was conducted and 58 contributions were finally found and selected. 28 of those contributions (48%) include a review of the existing models in the literature. Selected contributions include 46 journal papers, 5 books, 2 Ph.D. Thesis, 2 communications published in conference proceedings and 3 technical reports. All contributions were written in English but one, that was published in Spanish.
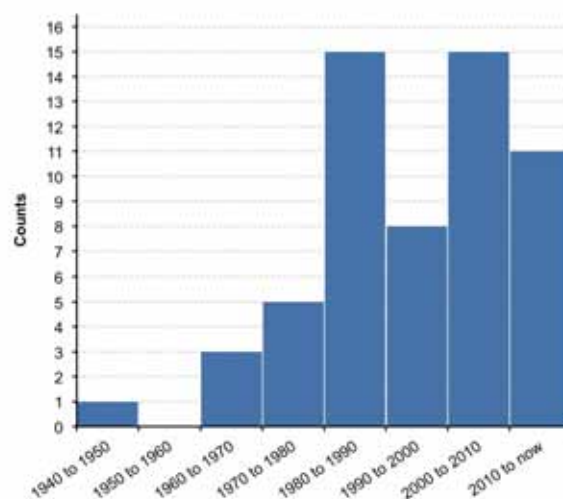
Figure 2: Histogram of the reviewed contributions grouped by their publication dates.

Figure 2 shows an histogram of the analysed contributions grouped by the decades of the publication dates. It can be observed that almost the 45% of the references are subsequents to the 2000s. Thus, balance between

6

original sources of the models' descriptions and the latest reviews in the field has been guaranteed.

Focusing on the reviewed journal papers, to assure their quality and international validation, in addition to considering only indexed international journals, a citation analysis has been conducted. Results are shown in Table 2. In this analysis, references [50] and [51] have been discarded because of, due to the wide interdisciplinarity of the application of the described nonparametric models, they achieve a number of citations out of bounds: 3 796 and 12 082 respectively.

Table 2: Citation analysis of the selected journal papers. Number of citations from Google Scholar database.

| Parameter | Value |
|-----------|-------|
| Count | 43 |
| Mean | 108.72 |
| Min. | 0 |
| Q1 | 15 |
| Median | 66 |
| Q3 | 134.5 |
| Max. | 554 |

With a mean number of citations of 108.72 and a median of 66, it is demonstrated that the selected references can be considered representative in the field and that they have been validated by the scientific community.

Finally, from those contributions wich include a review (either they are review works or because they include a review section or a comparison between different models performance) the average number of the reviewed models is 10.125, with a standard deviation of 5.669. The found most complete review work includes 26 models.

It has been found a wide range of models for determining the value of diffuse irradiance on an inclined plane oriented in an equatorial direction. The extension of the results of models for inclined planes with different orientations is brought about by considering the angle formed by the position of the Sun and the direction vector that characterises the studied surface. In this section, an exhaustive review of the existing and most widely used models is conducted.

Transpositon models range from the simplest formulations in the end of the 1940s to the most modern techniques based on soft computing. No standardised nomenclature for describing the models is observed; thus some original expressions have been modified to adapt them to an homogeneous nomenclature where appropriate. Moreover, according to their formulation and characteristics, models have been classified into two classes and four main groups (see Figure 3):

**Parametric models:** based on the integration of the differential radiance equation in the atmosphere. They can be parametrised. Depending on the radiance distribution hypothesis it can be distinguised isotropic or anisotropic models. Parametric models are the most widely extended in the literature.

**Isotropic models:** these consider a homogeneous distribution of radiance in the atmosphere. Thus, they are independent of the observed sky patch.

**Anisotropic superposition models:** they consider the effects of anisotropy in the circumsolar region and/or the horizontal band. They evaluate the total diffuse irradiance as the sum (or composition) of a background isotropic irradiance and one or two components that encompass the atmosphere's anisotropies.

**Relative radiance anisotropic models:** these models perform a comprehensive analysis of the angular distribution of radiance, parameterising it in accordance with the zenith and azimuth angles of the differential region of the sky analysed in each case. A gradient function describes the variance of the radiance with the zenith angle and an indicatrix function modifies radiance with the azimuth angle with respect a zenith radiance. Furthermore, models in this category can be classified into overcast sky, clear sky, intermediate sky or all-sky distributions. Let's notice that most classical isotropic and anisotropic models are particular results of the integration of relative radiance models, such as it can be demonstrated for the Liu & Jordan model considering a constant radiance flux, or for the Steven & Unsworth model considering a linearly variation with $\cos\theta_z$ [38]. Total diffuse irradiance is obtained by integrating the sky radiance through the observed sky vault. Thus, diffuse irradiance on a tilted surface may be expressed as:

$$D(\theta_{zp}, \gamma_p) = \int_{\gamma_p - \pi/2}^{\gamma_p + \pi_2} \int_0^{\pi/2} I(\theta_z, \gamma)\cos\xi_p \sin\theta_z d\theta_z d\gamma$$
$$+ \int_{\gamma_p + \pi/2}^{\gamma_p + 3\pi/2} \int_0^{\theta_{z\gamma}} I(\theta_z, \gamma)\cos\xi_p \sin\theta_z d\theta_z d\gamma, \quad (7)$$

where the integration limit $\theta_{z\gamma}$ is the zenith angle of the intersection of the surface with the sky dome
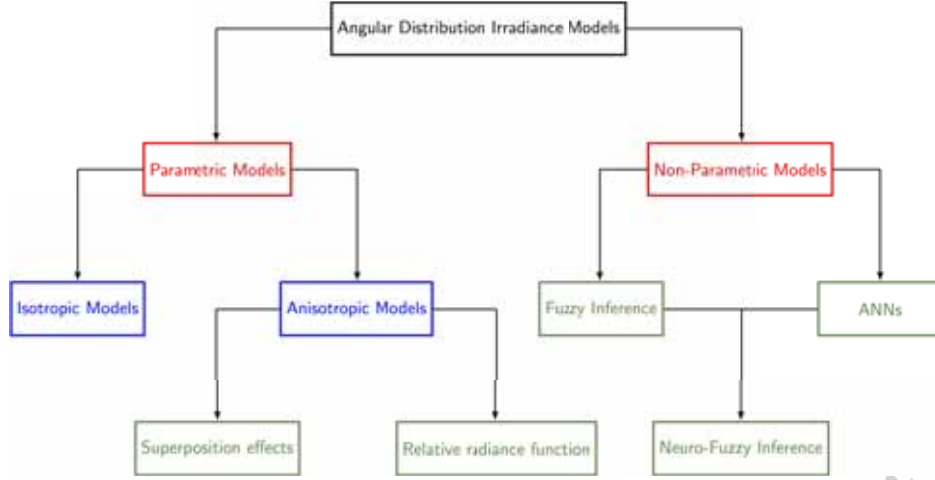
7

Figure 3: Solar diffuse irradiance transposition models classification.

and $\xi_p$ the angle between a point in the sky and the sensor. Radiance function, $I(\theta_z, \gamma)$, is expressed as the product of the zenith radiance, $I_z$, and the relative radiance function $i_r(\theta_z, \gamma)$:

$$I(\theta_z, \gamma) = i_r(\theta_z, \gamma)I_z. \qquad (8)$$

Zenith radiance can be obtained from the measured diffuse irradiance on the horizontal plane:

$$I_z = \frac{D(0)}{\displaystyle\int_0^{2\pi}\int_0^{\pi/2} i_r(\theta_z, \gamma)\cos\theta_z\sin\theta_z d\theta_z d\gamma}. \qquad (9)$$

Similarly, albedo's irradiance in this sort of models can be expressed as:

$$R(\theta_{zp}, \gamma_p) = \int_{\gamma_p-\pi/2}^{\gamma_p+\pi/2}\int_{\pi/2}^{\pi-\theta_{z\gamma}} I_g(\theta_z, \gamma)\cos\xi_p\sin\theta_z d\theta_z d\gamma, \qquad (10)$$

where $I_g(\theta_z, \gamma)$ is the albedo's radiance, which also could be defined as the product of a relative radiance function, $i_{gr}(\theta_z, \gamma)$, and a nadith radiance, $I_{gz}$. In this work, albedo's radiance is supossed to be isotropic, thus:

$$I_g(\theta_z, \gamma) = i_{gr}(\theta_z, \gamma)I_{gz} = \frac{\rho G(0)}{\pi}. \qquad (11)$$

**Non-parametric models:** this class includes models that are not based on physical hypothesis but allow

the adjustment between input variables or estimators and output variables or responses. Although several techniques exist in this field, the most extended models in recent decades are based on automated learning or soft computing. These algorithms, which most of them mimic human inference processes, are powerful tools and some of them can perform as universal aproximators of any unknown function. The best results on transposition models seem to have been obtained by fuzzy inference systems, artificial neural networks and neuro-fuzzy networks.

**Fuzzy inference models:** fuzzy models are based on the fuzzy sets theory and allow to map inputs to outputs. Two main alternatives of these models can be found: the Mamdani-type fuzzy inference and the Takagi-Sugeno fuzzy inference.

**Artificial Neural Networks:** ANNs are a family of models inspired by biological neural networks and can be used wether to classify data or to approximate functions. For transposition problems, only universal approximators ANNs can be used. They may differ on the architecture, the activity rule or the learning rule or learning paradigm. Many versions of the ANNs have been developed through the recent decades, outstanding the Multi-Layer Perceptron, the Radial Basis Function based ANN and the Generalised Regression Neural Network.

**Neuro-fuzzy networks:** these combine the fuzzy inference techniques with the structure of artificial neural networks. They are based on backforward net-

8

works which activation functions are modelised according to fuzzy sets theory. The most extended model in this category is the ANFIS model, developed by Jang in 1993. Several versions of it can be found since then applied to several engineering and science fields.

Table 3: Analysed diffuse irradiance models for tilted surfaces. Column "Type" classifies the models, column "Ref" includes the original and/or descriptive references in the literature and column "ID" assigns an identifier to each model.

| Type | Model | Ref | ID |
|------|-------|-----|-----|
| **Parametric models** | | | |
| Isotropic | Liu & Jordan | [52] | D01 |
| | Tian et al. | [33] | D02 |
| | Badescu | [53] | D03 |
| | Koronakis | [54] | D04 |
| | Olmo | [55, 34, 56] | D05 |
| Anisotropic superposition | ASHRAE | [57] | D06 |
| | Díez-Mediavilla | [58] | D07 |
| | DOE-2 | [59] | D08 |
| | Gueymard | [60, 61] | D09 |
| | Hay & Davies | [62, 63] | D10 |
| | Klucher | [64] | D11 |
| | Ma & Iqbal | [65] | D12 |
| | Muneer | [66, 67] | D13 |
| | Perez et al. | [68, 32] | D14 |
| | Perez et al. opt. | [68, 32] | D15 |
| | Reindl | [69] | D16 |
| | Skartveit & Olseth | [70, 71] | D17 |
| | Steven & Usworth | [72, 73] | D18 |
| | Temps & Coulson | [74] | D19 |
| | Willmott | [75] | D20 |
| Anisotropic relative radiance | Brunger & Hooper | [76] | D21 |
| | CIE 2004 | [38] | D22 |
| | TCCD | [77] | D23 |
| | Igawa et al. | [78, 79] | D24 |
| | Moon & Spencer | [80] | D25 |
| | Siala & Hooper | [81] | D26 |
| **Non-parametric models** | | | |
| Neural Networks | MLP | [82] | D27 |
| | RBF | [50] | D28 |
| | GRNN | [83] | D29 |
| Neuro-Fuzzy | ANFIS | [51] | D30 |

According to the proposed classification, 30 different models have been analysed and described. In Table 3 these models can be shown, classified according to proposed criteria. Other similar carried out studies in this field have compared only isotropic and anisotropic by superposition models [84, 85, 86, 87, 88]. Very few studies analyse in deep parametric and non-parametric models together. Moreover, the high computation requirements for the evaluation of anisotropic by gradient models (several complex integrations are needed) also exclude them from most studies.

Although more models of each category can be found, specially anisotropic by superposition models, a selection have been done according to the most widely extended, significantly different structure and/or characteristics and best obtained results.

The following sections describe used formulations for each model. It must be remarked that mistakes on shown formulations in some papers have been propagated in the literature. Some authors have tried to fix them in their reviews [87, 61], and so this work. Furthermore, a standardised formulation for common variables is used here, which may differ from the original.

Transposition models are based on the hypothesis of that total or global irradiance on a tilted and oriented plane, $G(\theta_{zp}, \gamma_p)$, where $\theta_{zp}$ is the zenith angle of the pyranometer or sensor and $\gamma_p$ its azimuth angle (0 rad for the South direction, East negative), can be estimated as the sum of the irradiance components,

$$G(\theta_{zp}, \gamma_p) = R_b B(0) + R_d D(0) + R_r \rho G(0). \quad (12)$$

In this work, it has been defined as $R_d$ the transposition relation between the horizontal diffuse irradiance and the tilted diffuse irradiance,

$$R_d = \frac{D(\theta_{zp}, \gamma_p)}{D(0)}. \quad (13)$$

Similarly, $R_r$ is defined as the transposition relation between the reflected horizontal global irradiance by the surroundings and the reflected irradiance measured on the tilted surface,

$$R_r = \frac{R(\theta_{zp}, \gamma_p)}{\rho G(0)}, \quad (14)$$

where $\rho$ is the reflectance of the surroundings which can be specifically measured by an albedometer or estimated as function of the reflecting material [38].

Most authors consider $R_r$ under an isotropic distribution hypothesis. Thus, equation 15 is usually considered. In following sections, this parameter formula will be only specified for those models which consider other hypothesis for reflected irradiance distribution.

$$R_r = \frac{1 - \cos\theta_{zp}}{2}. \quad (15)$$

For tilted diffuse irradiance measurement on tilted and oriented planes, reflected irradiance can be avoided

by installing an appropriate shield to block irradiance incidence from the ground. However, these devices also obstruct the sensor and interferences in the measurements can be obtained.

### 3.1. Liu & Jordan (D01)

This model, presented in [52], is one of the most extended in the bibliography and it can be obtained by the integration of the sky radiance under the isotropic hypothesis where $i_r(\theta_z, \gamma) = 1$.

$$R_d = \frac{1 + \cos \theta_{zp}}{2}. \tag{16}$$

### 3.2. Tian et al. (D02)

In [33], the diffuse and reflected contributions of the irradiance incident on a tilted plane are proportional to the observed sky vault by the surface, which differ slightly from the Liu & Jordan model (D01).

$$R_d = \frac{\pi - \theta_{zp}}{\pi}, \tag{17}$$

$$R_r = \frac{\theta_{zp}}{\pi}. \tag{18}$$

### 3.3. Badescu (D03)

This model is characterized by the ponderation of the zenith angle of the incoming radiance on the surface.

$$R_d = \frac{3 + \cos(2\theta_{zp})}{4}, \tag{19}$$

$$R_r = \frac{1 - \cos(2\theta_{zp})}{4}. \tag{20}$$

### 3.4. Koronakis (D04)

Similarly to model D03, in [54] is proposed a model which ponderates the origin of the sky radiance (63% of the irradiance is considered to come from the equatorial hemisphere of the observed sky vault). However, the reflected irradiance is considered to be isotropic.

$$R_d = \frac{2 + \cos \theta_{zp}}{3}. \tag{21}$$

### 3.5. Olmo (D05)

$$R_d = \frac{G(0) \exp\left[-k_t\left(\xi_{sp}^2 - \theta_{zs}^2\right)\right] - R_b B(0)}{D(0)}, \tag{22}$$

where $k_t$ is the clearness index and $\xi_{sp}$ is the angle between the sun's position and the pyranometer direction (**p** vector).

In the original reference [55] where this model is proposed, the definition of $\xi_{sp}$ results geometrically incorrect [34] and, thus, equation 23 must be applied.

$$\begin{aligned}
\cos \xi_{sp} = {} & \sin \phi_g \sin \delta_s \cos \theta_{zp} - \cos \phi_g \sin \delta_s \sin \theta_{zp} \cos \gamma_p \\
& + \cos \phi_g \cos \delta_s \cos \omega_s \cos \theta_{zp} \\
& + \sin \phi_g \cos \delta_s \cos \omega_s \sin \theta_{zp} \cos \gamma_p \\
& + \cos \delta_s \sin \omega_s \sin \theta_{zp} \sin \gamma_p.
\end{aligned} \tag{23}$$

In this expression, $\phi_g$ is the geographical latitude.

The reflected irradiance component can be also extracted from the original model:

$$R_r = \exp\left[-k_t\left(\xi_{sp}^2 - \theta_{zs}^2\right)\right] \sin^2\left(\frac{\xi_{sp}}{2}\right). \tag{24}$$

Because of found significant deviations with real measurements [87], some authors proposed modified expressions [56]:

$$R_r = \begin{cases} -\exp\left[-k_t\left(\xi_{sp}^2 - \theta_{zs}^2\right)\right]\cos^3\left(\dfrac{\xi_{sp}}{2}\right) & \text{if } 0 \le k_t < 0.35, \\[2ex] -\exp\left[-k_t\left(\xi_{sp}^2 - \theta_{zs}^2\right)\right]\sin\left(\dfrac{\xi_{sp}}{2}\right) & \text{if } 0.35 \le k_t \le 0.65. \end{cases} \tag{25}$$

### 3.6. ASHRAE (D06)

This model was initially proposed by the American Society of Heating, Refrigerating and Air-Conditioning Engineers from data gathered in USA and Canada. It has been adopted sucessive improvements through time and it has been recomended to be applied in computational simulations of buildings' thermal behaviours [57]. Explicit formula for $R_d$ can be found in [60]:

$$R_d = R_{dT} + \left(\frac{C_N^2}{C} - \frac{B(n)}{D(0)}\right)\rho R_r \cos \theta_{zs}, \tag{26}$$

where $R_{dT}$ is an empirical function developed in [89], $C$ is an empirical coefficient which is seasonally dependent and that can be calculated through a polinomic regression of the values given in [90] (see equation (28)

10

and Figure 4). $C_N$ is the so-called clarity index which value has only been established by ASHRAE for USA. $C_N = 1$ has been used in this study in absence of real measurements or estimations.

$$R_{dT} = \begin{cases} 0.45 & \text{if } \cos \xi_{sp} \leq 0.2, \\ 0.55 + 0.437 \cos \xi_{sp} & \\ + 0.313 \cos^2 \xi_{sp} & \text{if } \cos \xi_{sp} > 0.2. \end{cases} \quad (27)$$

$$C = a_0 + a_1 N + a_2 N^2 + a_3 N^3 + a_4 N^4 + a_5 N^5 + a_6 N^6, \quad (28)$$

where $N$ is the day of the year and coefficients $a_i$, with $i \in \{0, 1, 2, 3, 4, 5, 6\}$, have been calculated respectively as: $a_0 = 0.0530$, $a_1 = 5.6048\text{E-4}$, $a_2 = -2.2630\text{E-5}$, $a_3 = 3.8458\text{E-7}$, $a_4 = -2.3524\text{E-9}$, $a_5 = 5.9699\text{E-12}$, $a_6 = -5.4191\text{E-15}$.
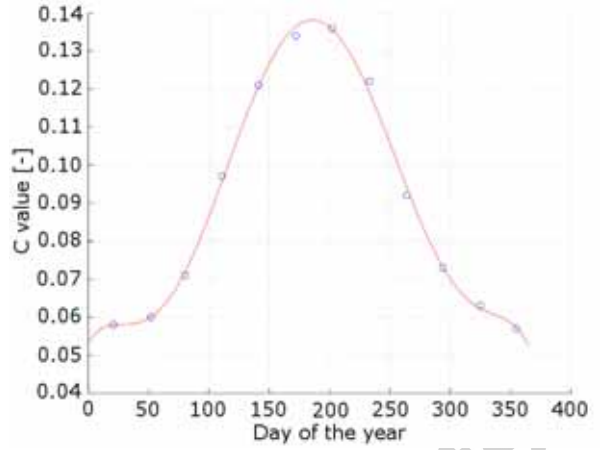


Figure 4: $C$ coefficient from Threlkeld.

### 3.7. Díez-Mediavilla (D07)

$$R_d = \frac{1 + \cos \theta_{zp}}{2} + N_1 N_2, \quad (29)$$

where $N_1$ is adjusted to the optimum value for any Perez et al's clearness index, $\varepsilon'$, and $N_2$ is a parameter depending on the zenith angle.

$$N_1 = \frac{2b}{\pi(3 + 2b)} = 0.0751 - 1.999 A_i - 0.8800 A_i^2, \quad (30)$$

where $b$ is the radiance sky distribution index, which theoretical limit is $b = 0$ (isotropic sky). Empirical studies state its value in the range $b \in [1.0, 2.0]$ [38]. $A_i$ is

the anisotropy index or modulation function defined by Hay & Davies in equation (49).

$$N_2 = \sin \theta_{zp} - \theta_{zp} \cos \theta_{zp} - \pi \frac{1 - \cos \theta_{zp}}{2}. \quad (31)$$

### 3.8. DOE-2 (D08)

This model is implemented in several simulation computer programs, such as DOE-2 and ENCORE-CANADA.

$$R_d = \begin{cases} 1 & \text{if } \theta_{zp} < 45°, \\ R_{dT} & \text{if } 45° \leq \theta_{zp} < 135°, \\ 0 & \text{if } \theta_{zp} \geq 135°. \end{cases} \quad (32)$$

$R_{dT}$ has been defined in equation (27).

### 3.9. Gueymard (D09)

$$R_d = (1 - N_G)R_{d0} + N_G R_{d1}, \quad (33)$$

where the 0 subindex refers to clear sky conditions and 1 subindex to a cover sky. $R_{d0}$ is calculated through the following regression expression:

$$R_{d0} = \exp\left(a_0 + a_1 \cos \xi_{sp} + a_2 \cos^2 \xi_{sp} + a_3 \cos^3 \xi_{sp}\right) + F1_G(\theta_{zp}) + F2_G(h'_s), \quad (34)$$

where coefficients $a_i$, with $i \in \{0, 1, 2, 3\}$, are functions of the corrected solar heigth $h'_s$, which is related with the solar heigth $h_s$ in degrees:

$$h'_s = 0.01 h_s, \quad (35)$$

$$h_s = 90 - \frac{180}{\pi} \theta_{zs}. \quad (36)$$

$$a_0 = -0.897 - 3.364 h'_s + 3.960 h'^2_s - 1.909 h'^3_s, \quad (37)$$

$$a_1 = 4.448 - 12.962 h'_s + 34.601 h'^2_s - 48.784 h'^3_s + 27.511 h'^4_s, \quad (38)$$

$$a_2 = -2.770 + 9.164 h'_s - 18.876 h'^2_s + 23.776 h'^3_s - 13.014 h'^4_s, \quad (39)$$

$$a_3 = 0.312 - 0.217 h'_s - 0.805 h'^2_s + 0.318 h'^3_s. \quad (40)$$

Functions $F1_G(\theta_{zp})$ and $F2_G(h'_s)$ estimate the distribution of the background irradiance and are a function of the tilting angle and the corrected solar heigth respectively. $F1_G(\theta_{zp})$ is defined by:

$$F1_G(\theta_{zp}) = \frac{1 + b_0 \sin^2 \theta_{zp} + b_1 \sin\left(2\theta_{zp}\right) + b_2 \sin\left(4\theta_{zp}\right)}{1 + b_0}, \quad (41)$$

11

where coefficients $b_j$, with $j \in \{0, 1, 2\}$, are $b_0 = -0.2249$, $b_1 = 0.1231$ and $b_2 = -0.0342$. Expression for function $F2_G(h'_s)$ is:

$$F2_G(h'_s) = 0.408 - 0.323h'_s + 0.384h_s^{'2} - 0.170h_s^{'3}. \quad (42)$$

On the other hand, $R_{d1}$ is defined as:

$$R_{d1} = \frac{1 + \cos\theta_{zp}}{2} + \frac{2b}{\pi(3 + 2b)}\left(\sin\theta_{zp} - \theta_{zp}\cos\theta_{zp}\right) - \frac{2b}{3 + 2b}\frac{1 - \cos\theta_{zp}}{2}, \quad (43)$$

Although the sky distribution index value varies locally, Gueymard estimates a global mean value $b = 1.5$ for totally covered skies and $b = 0.5 + N_G$ for clear and partially covered ones.

$$N_G = \max\{\min[Y(k_d), 1], 0\}, \quad (44)$$

where function $Y(k_d)$ is defined for two diffuse fraction ranges:

$$Y(k_d) = \begin{cases} 6.6667k_d - 1.4167 & \text{si } k_d \leq 0.227, \\ 1.2121k_d - 0.1758 & \text{si } k_d > 0.227. \end{cases} \quad (45)$$

Finally, for specular surfaces:

$$R_r = f_b\frac{\rho_b}{\rho}\frac{B(n)\cos\xi_{gp}}{G(0)} + \frac{\rho_d}{\rho}\frac{1 - \cos\theta_{zp}}{2}k_d, \quad (46)$$

where $\rho$ is the apparent reflectance of the surroundings (usually $\rho = 0.2$). $f_b$ is a shadowing coefficient which value is $f_b = 1$ where no obstacles shadow the direct beam irradiance and $f_b = 0$ for total shadowing. For partial shadowing its value must be determined empirically. $\xi_{gp}$ is the incident angle of the reflected irradiance on the tilting surface, which can be calculated through the following expression:

$$\cos\xi_{gp} = \sin\theta_{zp}\sin\theta_{zs}\cos\left(\gamma_s - \gamma_p\right) - \cos\theta_{zp}\cos\theta_{zs}. \quad (47)$$

### 3.10. Hay & Davies (D10)

$$R_d = A_iR_b + (1 - A_i)\frac{1 + \cos\theta_{zp}}{2}. \quad (48)$$

$A_i$ is the anisotropy index or modulation function. It is defined in the same terms than the diffuse function $F$:

$$A_i = F = \frac{G(0) - D(0)}{B_{ext}(0)} = \frac{B(0)}{B_{ext}(0)}, \quad (49)$$

where the horizontal extraterrestial irradiance $B_{ext}(0)$ can be approximated by:

$$B_{ext}(0) = B_{sc}[1 + 0.033\cos(0.017202N)]\cos\theta_{zs}. \quad (50)$$

### 3.11. Klucher (D11)

$$R_d = \frac{1 + \cos\theta_{zp}}{2}\left[1 + A_i^K\sin^3\left(\frac{\theta_{zp}}{2}\right)\right]\left(1 + A_i^K\cos^2\theta_{sp}\sin^3\theta_{zs}\right), \quad (51)$$

where $A_i^K$ is the particular definition of the anisotropy index or modulation function defined by the expression:

$$A_i^K = 1 - \left[\frac{D(0)}{G(0)}\right]^2 = 1 - k_d^2. \quad (52)$$

### 3.12. Ma & Iqbal (D12)

$$R_d = k_t\cos\theta_{sp} + (1 - k_t)\frac{1 + \cos\theta_{zp}}{2}, \quad (53)$$

where $k_t$ is the clearness index.

### 3.13. Muneer (D13)

This model is defined for a sunlit surface under non-overcast sky:

$$R_d = T_M(1 - A_i) + A_iR_b, \quad (54)$$

where $T_M$ is a radiance distribution function defined by the author.

The Muneer's radiance distribution function is defined by:

$$T_M = \frac{1 + \cos\theta_{zp}}{2} + \frac{2b}{\pi(3 + 2b)}\left(\sin\theta_{zp} - \theta_{zp}\cos\theta_{zp}\right) - \frac{2b}{3 + 2b}\sin^2\left(\frac{\theta_{zp}}{2}\right), \quad (55)$$

where $\theta_{zp}$ must be introduced in [rad].

In equation (55), parameter $b$ is the radiance distribution index, proposed for the first time in [80] and lately analysed by other authors [91]. Muneer states its value to $b = 5.73$, for surfaces with no direct beam irradiance, and $b = 1.68$ for the rest [66, 92]. As global average, $b = 2.5$ is acepted for covered sky conditions. For clear skies, the author propose the following expression:

12

$$\frac{2b}{\pi(3 + 2b)} = 0.0400 - 0.820A_i - 2.026A_i^2. \quad (56)$$

Nevertheless, for South European locations, the authors advise to use the following equation (validated for Geneve and Switzerland):

$$\frac{2b}{\pi(3 + 2b)} = 0.00263 - 0.712A_i - 0.6883A_i^2. \quad (57)$$

This last expression is the one applied in the current work as it results more precise to the measurement location.

### 3.14. Perez et al. (D14)

In 1983 Perez et al. propose a model based in the superposition of the isotropic background diffuse irradiance, circunsolar component and horizon brightening which is then optimised in [68, 32]. Final version from 1990 [32] is used in this work:

$$R_d = (1 - F_1) \frac{1 + \cos \theta_{zp}}{2} + F_1 R_b + F_2 \sin \theta_{zp}, \quad (58)$$

where $F_1$ and $F_2$ are the circunsolar and horizon brightening coefficients respectively. Coefficients $F_1$ and $F_2$ are defined as a function of the zenith angle ($\theta_{zs}$), the Perez's clearness index ($\varepsilon$) and the sky brightness index ($\Delta$), described in equations (61) and (62) respectively.

$$F_1 = \max(F_{11} + \Delta F_{12} + \theta_{zs} F_{13}, 0), \quad (59)$$

$$F_2 = F_{21} + \Delta F_{22} + \theta_{zs} F_{23}, \quad (60)$$

where the zenith angle $\theta_{zs}$ is measured in [rad]. Average global values for coefficients $F_{ij}$ are given by Perez et al. in Table 4.

$$\varepsilon = \frac{\frac{D(0) + B(n)}{D(0)} + k\theta_{zs}^3}{1 + k\theta_{zs}^3}. \quad (61)$$

In equation (61) $k = 1.041$ for $\theta_{zs}$ measured in [rad].

$$\Delta = \frac{mD(0)}{B_{ext}(n)}. \quad (62)$$

The optical air mass, $m$, is defined by Kasten in [93]:

$$m = \frac{p}{p_0} \frac{1}{\sin h_s + 0.00176759(94.37515 - h_s)^{-1.21563}}, \quad (63)$$

where $p$ is the site's atmospheric pressure in [mbar] and $p_0 = 1\,013.25$ mbar.

### 3.15. Perez et al. opt. (D15)

Coefficients $F_{ij}$ can be locally optimized or fitted. The following procedure has been applied to calculate the locally fitted coefficients:

1. For the training dataset the Perez's clearness index ($\varepsilon$), the brightness index ($\Delta$), the Kasten's optic relative air mass ($m$) and the zenith angle ($\theta_{zs}$) are calculated.
2. The dataset is divided in 8 intervals according to the $\varepsilon$ value.
3. For each interval, a multi-parameter regression is conducted guaranteeing the normality and the homocedasticity of the residuals. Thus, the absolute value of the studentized residuals is observed to be less than 2. Linear regression expression is obtained by rearranging terms in equation (58):

$$R_d - \frac{1 + \cos \theta_{zp}}{2} = \left(R_b - \frac{1 + \cos \theta_{zp}}{2}\right) F_1 + \sin \theta_{zp} F_2. \quad (64)$$

If we define $R_d - (1 + \cos \theta_{zp})/2 = y$, $R_b - (1 + \cos \theta_{zp})/2 = a_0$ and $\sin \theta_{zp} = a_1$, then it is obtained:

$$y = a_0 F_1 + a_1 F_2. \quad (65)$$

Expressions (59) and (60) are introduced in the previous equation:

$$y = a_0 \max(b_0 + \Delta b_1 + \theta_{zs} b_2, 0) + a_1(b_3 + \Delta b_4 + \theta_{zs} b_5),$$
$$(66)$$

or in a matrix form ($\forall (b_0 + \Delta b_1 + \theta_{zs} b_2) \geq 0$):

$$y = (b_0, b_1, b_2, b_3, b_4, b_5) \cdot \begin{pmatrix} a_0 \\ a_0 \Delta \\ a_0 \theta_{zs} \\ a_1 \\ a_1 \Delta \\ a_1 \theta_{zs} \end{pmatrix} = \mathbf{b} \cdot \mathbf{x}. \quad (67)$$

Vector's components $\mathbf{b}$ result to be coefficients $F_{ij}$ from the model. Thus, regression of $\mathbf{y}$ over $\mathbf{x}$ is carried out.

Results of the optimization are shown in Tables 5, 6, 7 and 8. In these tables, parameter $n$ is the dataset size.

### 3.16. Reindl (D16)

$$R_d = (1 - A_i) \frac{1 + \cos \theta_{zp}}{2} \left[1 + A_i^R \sin^3\left(\frac{\theta_{zp}}{2}\right) + A_i R_b\right]. \quad (68)$$

13

Table 4: Perez et al.'s proposed coefficients for diffuse irradiance calculation. Source: [32].

| $\varepsilon$ | $\mathbf{F_{11}}$ | $\mathbf{F_{12}}$ | $\mathbf{F_{13}}$ | $\mathbf{F_{21}}$ | $\mathbf{F_{22}}$ | $\mathbf{F_{23}}$ |
|---|---|---|---|---|---|---|
| [1.000, 1.065) | −0.0083 | 0.5877 | −0.0621 | −0.0596 | 0.0721 | −0.0220 |
| [1.065, 1.230) | 0.1299 | 0.6826 | −0.1514 | −0.0189 | 0.0660 | −0.0289 |
| [1.230, 1.500) | 0.3297 | 0.4869 | −0.2211 | 0.0554 | −0.0640 | −0.0261 |
| [1.500, 1.950) | 0.5682 | 0.1875 | −0.2951 | 0.1089 | −0.1519 | −0.0140 |
| [1.950, 2.800) | 0.8730 | −0.3920 | −0.3616 | 0.2256 | −0.4620 | 0.0012 |
| [2.800, 4.500) | 1.1326 | −1.2367 | −0.4118 | 0.2878 | −0.8230 | 0.0559 |
| [4.500, 6.200) | 1.0602 | −1.5999 | −0.3589 | 0.2642 | −1.1272 | 0.1311 |
| [6.200, ∞) | 0.6777 | −0.3273 | −0.2504 | 0.1561 | −1.3765 | 0.2506 |

Table 5: Locally fitted Perez et al.'s coefficients for the North direction.

| $\varepsilon$ | $\mathbf{F_{11}}$ | $\mathbf{F_{12}}$ | $\mathbf{F_{13}}$ | $\mathbf{F_{21}}$ | $\mathbf{F_{22}}$ | $\mathbf{F_{23}}$ | $\mathbf{n}$ |
|---|---|---|---|---|---|---|---|
| [1.000, 1.065) | 4.916 | 0.170 | −3.304 | 2.533 | −0.204 | −1.649 | 2 529 |
| [1.065, 1.230) | 3.670 | −0.844 | −2.194 | 1.810 | −0.887 | −0.923 | 461 |
| [1.230, 1.500) | 26.01 | −15.58 | −15.34 | 12.98 | −8.394 | −7.430 | 294 |
| [1.500, 1.950) | 8.119 | −1.622 | −5.151 | 4.035 | −1.466 | −2.259 | 287 |
| [1.950, 2.800) | 14.26 | −4.796 | −9.291 | 7.066 | −3.400 | −4.136 | 362 |
| [2.800, 4.500) | −11.52 | −2.111 | 7.966 | −5.700 | −3.731 | 4.783 | 407 |
| [4.500, 6.200) | −29.13 | 83.10 | 12.25 | −14.25 | −11.47 | −1.402 | 344 |
| [6.200, ∞) | 0.000 | 0.000 | 0.000 | 0.777 | −16.34 | 1.853 | 352 |

Table 6: Locally fitted Perez et al.'s coefficients for the South direction.

| $\varepsilon$ | $\mathbf{F_{11}}$ | $\mathbf{F_{12}}$ | $\mathbf{F_{13}}$ | $\mathbf{F_{21}}$ | $\mathbf{F_{22}}$ | $\mathbf{F_{23}}$ | $\mathbf{n}$ |
|---|---|---|---|---|---|---|---|
| [1.000, 1.065) | 0.026 | 0.515 | −0.096 | −0.048 | 0.463 | −0.060 | 2 353 |
| [1.065, 1.230) | 0.268 | 0.268 | −0.123 | 0.275 | −0.196 | −0.090 | 319 |
| [1.230, 1.500) | 0.097 | 0.239 | 0.051 | 0.548 | −0.986 | −0.070 | 253 |
| [1.500, 1.950) | 0.663 | 0.035 | −0.303 | 0.406 | −1.015 | 0.105 | 311 |
| [1.950, 2.800) | 0.831 | 0.180 | −0.449 | 0.459 | −1.804 | 0.304 | 306 |
| [2.800, 4.500) | 0.656 | 0.509 | −0.294 | 0.146 | −0.373 | −0.034 | 467 |
| [4.500, 6.200) | −2.264 | 7.269 | 1.238 | 0.261 | −2.832 | 0.558 | 210 |
| [6.200, ∞) | −6.399 | −1.200 | 6.256 | 2.002 | −5.796 | −0.925 | 346 |

Table 7: Locally fitted Perez et al.'s coefficients for the East direction.

| $\varepsilon$ | $\mathbf{F_{11}}$ | $\mathbf{F_{12}}$ | $\mathbf{F_{13}}$ | $\mathbf{F_{21}}$ | $\mathbf{F_{22}}$ | $\mathbf{F_{23}}$ | $\mathbf{n}$ |
|---|---|---|---|---|---|---|---|
| [1.000, 1.065) | −0.180 | 0.674 | 0.065 | −0.036 | 0.161 | 0.056 | 2 533 |
| [1.065, 1.230) | 0.760 | 0.148 | −0.432 | 0.436 | −0.502 | −0.086 | 382 |
| [1.230, 1.500) | 1.288 | −0.023 | −0.776 | 0.694 | −0.532 | −0.278 | 259 |
| [1.500, 1.950) | 1.596 | −0.380 | −0.884 | 0.893 | −0.755 | −0.349 | 198 |
| [1.950, 2.800) | 1.724 | −1.244 | −0.766 | 0.913 | −1.765 | 0.014 | 358 |
| [2.800, 4.500) | 2.784 | −6.428 | −0.946 | 1.175 | −6.576 | 0.268 | 446 |
| [4.500, 6.200) | 2.826 | −9.515 | −1.014 | 1.135 | −7.987 | 1.023 | 422 |
| [6.200, ∞) | 1.757 | −7.971 | −0.340 | 0.901 | −8.413 | 1.015 | 398 |

14

Table 8: Locally fitted Perez et al.'s coefficients for the West direction.

| $\varepsilon$ | $F_{11}$ | $F_{12}$ | $F_{13}$ | $F_{21}$ | $F_{22}$ | $F_{23}$ | n |
|---|---|---|---|---|---|---|---|
| [1.000, 1.065) | 0.000 | 0.405 | −0.040 | 0.205 | 0.060 | −0.188 | 2 593 |
| [1.065, 1.230) | 0.454 | 0.191 | −0.251 | 0.440 | −0.344 | −0.208 | 409 |
| [1.230, 1.500) | 0.727 | 0.011 | −0.343 | 0.433 | −0.526 | −0.077 | 270 |
| [1.500, 1.950) | 0.731 | −0.058 | −0.304 | 0.335 | −0.440 | 0.052 | 234 |
| [1.950, 2.800) | 0.987 | −0.501 | −0.507 | 0.522 | −1.278 | 0.106 | 321 |
| [2.800, 4.500) | 0.103 | 6.398 | −1.116 | 0.188 | −0.171 | 0.204 | 394 |
| [4.500, 6.200) | −1.381 | 17.82 | −0.882 | −1.018 | 1.824 | 1.309 | 393 |
| [6.200, ∞) | −3.842 | 35.81 | −0.257 | −1.217 | 9.590 | 0.505 | 274 |

Particular anisotropy index, $A_i^R$, is described by:

$$A_i^R = \sqrt{\frac{B(0)}{G(0)}} = \sqrt{k_b}. \tag{69}$$

### 3.17. Skartveit & Olseth (D17)

$$R_d = A_i R_b + A_i^S \cos\theta_{zp} + (1 - A_i - A_i^S)\frac{1 + \cos\theta_{zp}}{2}, \tag{70}$$

where $A_i^S$ is the Skartveit & Olseth's modified modulation function or anisotropy index an it is defined by:

$$A_i^S = \max\left[(0.3 - 2A_i), 0\right]. \tag{71}$$

This model can be only applied if $A_i \geq 0.15$ is verified.

Furthermore, notice that in case there exist obstacles in the horizon, the following expression is proposed:

$$R_d' = -\int \frac{1 - A_i - A_i^S}{\pi} \cos\xi_{sp}\cos\xi_{op}\sin\xi_{op}d\xi_{op}, \tag{72}$$

where $\xi_{op}$ is the zenith angle between the obstacle in the observed sky vault and the surface direction (defined by vector **p**).

### 3.18. Steven & Unsworth (D18)

$$R_d = s_c R_b + \frac{1 + \cos\theta_{zp}}{2}$$
$$+ \frac{2b}{\pi(3 + 2b)}\left[\sin\theta_{zp} - \theta_{zp}\cos\theta_{zp} - \pi\sin^2\left(\frac{\theta_{zp}}{2}\right)\right]. \tag{73}$$

The first term in equation (73) quantifies the irradiance from the circumsolar region, which is considered in this model proportional to the diffuse irradiance,

and the rest quantifies the background irradiance. For a zenith angle in the range $[35°, 65°]$, authors propose $s_c = 0.51 \pm 0.02$ and $b = -0.87 \pm 0.07$, as general approach. The azimuth angle is measured in [rad].

It must be taken into account that if this model is applied to diffuse irradiance measures from shadowing devices (shadowband or shadowdisc mounted on a suntracker) the circumsolar component of the diffuse irradiance can not be measured and then, factor $s_c$ must be modified:

$$s_c' = \frac{s_c - f_c}{1 - f_c}, \tag{74}$$

where $f_c$ is the fraction of the circumsolar region blocked by the shadowing device.

### 3.19. Temps & Coulson (D19)

$$R_d = \frac{1 + \cos\theta_{zp}}{2}f_1 f_2, \tag{75}$$

where coefficients $f_1$ and $f_2$ are defined as following:

$$f_1 = 1 + \cos^2\theta_{sp}\sin^3\theta_{zs}. \tag{76}$$

$$f_2 = 1 + \sin^3\left(\frac{\theta_{zp}}{2}\right). \tag{77}$$

In this model, Temps and Coulson propose the following expression for the ground reflected irradiance, espcially validated for a grass environment:

$$R_r = \frac{1 - \cos\theta_{zp}}{2}\left[1 + \sin^2\left(\frac{\theta_{zs}}{2}\right)\right]\sin^2\theta_{zs}. \tag{78}$$

15

### 3.20. Willmott (D20)

$$R_d = \frac{A_i^W}{\cos \theta_{zp}} + C(\theta_{zp}) \left( 1 - \frac{A_i}{\cos \theta_{zp}} \right), \qquad (79)$$

where $A_i^W$ is the Willmott's modulation function or modified anisotropy index, defined as:

$$A_i^W = \frac{B(n) \cos \theta_{sp}}{B_{sc}}. \qquad (80)$$

Function $C(\theta_{zp})$ is the Revfeim integration of the associated geometry to the diffuse irradiance on a tilted surface [94], which can be approximated by:

$$C(\theta_{zp}) = 1.0115 - 0.20293\theta_{zp} - 0.080823\theta_{zp}^2, \quad (81)$$

where $0.5 \leq C(\theta_{zp}) \leq 1.0$; and $\theta_{zp}$ is measured in [rad].

This model also offers a modified expression for the transposition of the reflected irradiance:

$$R_r = \left( 1 + \frac{1 - \cos \theta_{zs}}{2} \right) |\cos(\gamma_s - \gamma_p)| \rho \frac{1 - \cos \theta_{zp}}{2}. \quad (82)$$

### 3.21. Brunger & Hooper (D21)

This model describes the spatial distribution of solar radiance as:

$$\frac{I(\theta_z, \xi_s)}{D(0)} = \frac{a_0 + a_1 \cos \theta_z + a_2 \exp(-a_3 \xi_s)}{\pi(a_0 + 2a_1/a_3) + 2a_2 J(\theta_{zs}, a_3)}, \quad (83)$$

where the coefficients $a_i$, with $i \in \{0, 1, 2, 3\}$, are calculated through the horizontal clearness index, $k_t$, and the diffuse fraction, $k_d$, depending on the sky conditions. Their values are tabulated in [76]. $\xi_s$ is the angle between a point in the sky and the Sun's position. The gradient function $J(\theta_{zs}, a_3)$ is defined as:

$$J(\theta_{zs}, a_3) = \frac{1 + \exp(-a_3\pi/2)}{a_3^2 + 4} \left[ \pi - f_a(a_3) f_b(\theta_{zs}) \right], \quad (84)$$

where $\theta_{zs}$ is expressed in [rad], and functions $f_a(a_3)$ and $f_b(\theta_{zs})$ are defined as follows:

$$f_a(a_3) = 1 - \frac{2}{\pi a_3} \frac{1 - \exp(-a_3\pi)}{1 + \exp(-a_3\pi/2)}. \qquad (85)$$

$$f_b(\theta_{zs}) = 2\theta_{zs} \sin \theta_{zs} - 0.02\pi \sin(2\theta_{zs}). \qquad (86)$$

### 3.22. CIE 2004 (D22)

This model is based on the Perez et al.'s all-weather model for luminance distribution in the sky dome. It is used by the International Commission of Luminance (CIE) to describe the standard general sky through the composition of a gradient and an indicatrix functions for the relative radiance:

$$i_r(\theta_z, \gamma) = \frac{f(\xi_s)g(\theta_z)}{f(\theta_{zs})g(0)}, \qquad (87)$$

where $f(\xi_s)$ is the indicatrix function, $g(\theta_z)$ is the zenith gradient function.

$$f(\xi) = 1 + c \left[ \exp(d\xi) - \exp\left(\frac{d\pi}{2}\right) \right] + e \cos^2 \xi. \quad (88)$$

$$g(\theta_z) = 1 + a \exp\left(\frac{b}{\cos \theta_z}\right). \qquad (89)$$

Coefficients $a$, $b$, $c$, $d$ and $e$ can define up to 36 different sky conditions. However, the standard model defined by CIE simplifies all combinations to just 15 sky types which coefficient values are tabulated in [95].

### 3.23. TCCD (D23)

This model, also called Hooper and Brunger (1980) model, expresses the irradiance function as:

$$\frac{I(\theta_z, \gamma)}{D(0)} = a_0 + a_1 \left(\frac{2\theta_z}{\pi}\right)^2 + a_2 \exp[-c\xi_s \exp(d\theta_{zs})], \quad (90)$$

where coefficients $a_0$, $a_1$ and $a_2$ cuantify the isotropic background radiance, the horizon brightening and the circumsolar anisotropic radiance. In absence of measurements, in [96] values for Toronto are offered. Coefficients $c$ and $d$ are constants that, according to [73], are estimated to $c = 0.0145423$ and $d = 0.0231798$ respectively.

### 3.24. Igawa et al. (D24)

This models adopts the same expression for $i_r(\theta, \gamma)$ than the CIE2004 model, shown in equation (87), but coefficients $a$, $b$, $c$ and $d$ are expressed as functions of the sky index Si instead of being tabulated.

$$a = \frac{4.5}{1 + 0.15 \exp(3.4\text{Si})} - 1.04. \qquad (91)$$

$$b = \frac{-1}{1 + 0.17 \exp(1.3\text{Si})} - 0.05. \qquad (92)$$

16

$$c = 1.77(1.22\text{Si})^{3.56} \exp(0.2\text{Si})(2.1 - \text{Si})^{0.8}. \quad (93)$$

$$d = \frac{-3.05}{1 + 10.6 \exp(-3.4\text{Si})}. \quad (94)$$

$$e = \frac{0.48}{1 + 245 \exp(-4.13\text{Si})}. \quad (95)$$

The sky index Si is defined by Igawa et al. as:

$$\text{Si} = \frac{G(0)}{G_{st}} + \sqrt{\text{Cle}}, \quad (96)$$

where $G_{st}$ is the standard global solar irradiance with a Linke turbidity of 2.5 and Cle is the cloudless index.

The expression to calculate $G_{st}$ is:

$$G_{st} = 0.84 \frac{B_{sc}}{m} \exp(-0.0675m), \quad (97)$$

$$\text{Cle} = \frac{1 - k_d}{1 - \text{Ces}}, \quad (98)$$

where Ces is the standard nubosity fraction, which can be obtained by a polynomic regression to the relative optical air mass:

$$\text{Ces} = 0.01299 + 0.07698m - 0.003857m^2 \\ + 0.0001054m^3 - 0.000001031m^4. \quad (99)$$

### 3.25. Moon & Spencer (D25)

This is one of the most classical models in this group and it describes the relative radiance as:

$$i_r(\theta_z) = \frac{1 + b \cos \theta_z}{1 + b}. \quad (100)$$

In [80], $b = 2$ was established for standard covered skies. Furthermore, this value is also adopted by the CIE standard with non-uniform nature for covered skies.

### 3.26. Siala & Hooper (D26)

This stochastic model proposed in 1987 express the sky radiance as:

$$I(\theta_z, \gamma) = \frac{a_1 a_2 B_{sc}}{4\pi \cos \theta_{zs}} \frac{1 - g^2}{(1 + g^2 - 2g \cos \xi_s)^{3/2}} \\ \left[ \delta_{\theta_z \theta_{zs}} f_1(\theta_{zs}) + (1 - \delta_{\theta_z \theta_{zs}}) f_2(\theta_z, \theta_{zs}) \right], \quad (101)$$

where $\delta_{\theta\theta_{zs}}$ is the Kroeneker's delta function for variables $\theta_z$ and $\theta_{zs}$, where, if $\theta_z = \theta_{zs}$, then $\delta_{\theta_z \theta_{zs}} = 1$, and

$\delta_{\theta_z \theta_{zs}} = 0$ otherwise. $f_1(\theta_{zs})$ and $f_2(\theta_z, \theta_{zs})$ are the following functions:

$$f_1(\theta_{zs}) = \exp\left(\frac{-a_2}{\cos \theta_{zs}}\right). \quad (102)$$

$$f_2(\theta_z, \theta_{zs}) = \exp\left(\frac{-a_2}{\cos \theta_z}\right) - \exp\left(\frac{-a_2}{\cos \theta_{zs}}\right). \quad (103)$$

Coefficients $a_1$ and $a_2$ can be obtained empirically by no-linear regression and $g$ is the asimetry factor of the phase function. Values for Toronto (Canada), which has similar latitude and weather conditions than the case study, are $a_1 = 1.287$, $a_2 = 0.460$ and $g = 0.438$, respectively [81]. These values have been adopted in the current study.

### 3.27. Multi-Layer Perceptron (D27)

MLP is an artificial neural network (ANN) which can operate as an universal approximator, in other words, it can approximate the output of any given function by its inputs and a training process. By using multiple layers, this model can be used to solve non-separable linear problems [97]. The architecture of the ANN is based on the model of neuron, firstly presented in [98] and lately modified in [99], where an input escalar $p_i$ is weighted by factor $w_i$, and a bias factor $b_i$ is added to the result:

$$n_i = w_i p_i + b_i. \quad (104)$$

In this model, $n_i$ is the network input to the transference or activation function $f_i(n_i)$, which produces the escalar output $a_i$ (see Figure 5). Multiple neurons in parallel form a layer. MLP model is characterized because the activation function is a sigmoid function, such as the log function, the hyperbolic tangent function or the identity function.

$$a_i(\mathbf{p}) = f_i(W \cdot \mathbf{p} + \mathbf{b}). \quad (105)$$

There exist several options to configure the MLP model for our purposes. In the case study, configuration of the MLP has been optimized by the Monte Carlo's method in such a way several combinations of input parameters and hidden layers have been compared. Results showed that the best configuration (lowest values of RMSD and MBD in training and validation datasets) must be the one shown in Table 9. The training dataset includes the 80% of the data and it is used for the supervised training of each configuration of the neural network. The validation dataset includes other 10% of the data and allows backpropagation. Finally each configuration performance is conducted through the results on
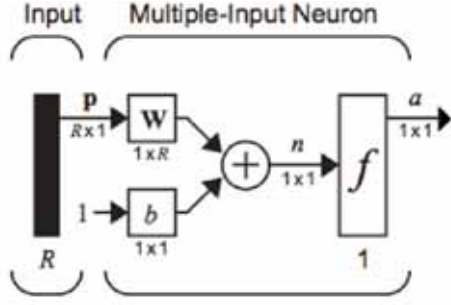
17

Figure 5: Multiple inputs neuron model. Adapted from [82].

the remaining 10% of the data (test dataset). To obtain a general model (avoiding overfitting), the previous optimization algorithm was applied to each cardinal direction and final model is obtained by a non-parametric aggregation procedure.

Table 9: MLP optimal configuration.

| Parameter | Value |
|-----------|-------|
| Inputs | $D(0)$, $G(0)$, $R(\theta_{zp})$, $\theta_{sp}$ |
| Outputs | $D(\theta_{zp}, \gamma_p)$ |
| Activation function | Logistic function |
| Hidden layers | 1 |
| Neurons in hidden layers | 5 |
| Training method | Lavenberg-Marquardt |
| Training epochs | 100 |
| Tolerance | 0.001 |

### 3.28. Radial Basis Function Neural Network (D28)

These ANNs are configurated as three layers feedforward networks with radial basis activation functions. This sort of functions calculate the euclidian distance of an input vector **p** with respect to a center $c_i$:

$$f_i(\mathbf{p}) = \|\mathbf{p} - c_i\|, \tag{106}$$

where each neuron in the hidden layer is associated to a radial basis function $\Phi(\|\mathbf{p} - c_i\|)$ and a weighting factor $w_i^k$:

$$a_i^k(\mathbf{p}) = \sum_{i=1}^{n} w_i^k \Phi_i(\|\mathbf{p} - c_i\|), \tag{107}$$

where $n$ is the number of neurons in the layer. Typical radial basis functions are the gaussian function, the

multicuadratic function and the inverse multicuadratic function.

The output layer makes a linear combination of the activated neurons in the hidden layer.

To achieve the optimal configuration, a similar procedure than the one followed for the MLP configuration was carried out. Results show that the best configuration must be the one expressed in Table 10.

Table 10: RBF optimal configuration.

| Parameter | Value |
|-----------|-------|
| Inputs | $D(0)$, $G(0)$, $R(\theta_{zp})$, $\theta_{sp}$ |
| Outputs | $D(\theta_{zp}, \gamma_p)$ |
| Activation function | Logistic function |
| Layers | 2 |
| Neurons in radial basis function layer | 150 |
| Training method | Bayesian regularization |
| Tolerance | 0.001 |

### 3.29. Generalised Regression Neural Network (D29)

This sort of ANNs are a particular case of radial basis function neural networks where the weighting matrix is obtained by applying an analytic method without training. Thus, it just needs one iteration to be trained or adapted [100]. These ANNs follow a feedforward algorithm and need supervised training. Moreover, the application of the risk bayesian criteria increases significantly their accuracy [101].

GRNNs are configured with two layers. The first one gets the inputs and includes the radial basis functions. It has got as many neurons as inputs-targets pairs in vector **p**. Bias value is asigned $0.8326/\sigma$, where $\sigma$ is the maximum amplitude of the radial basis function. The second layer has got the same number of neurons as the first one but it implements linear basis functions instead.

As shown before, an optimization algorithm has been applied to obtain the best results from the model. The final optimal configuration for the estimation of vertical diffuse irradiance on several cardinal directions is exposed in Table 11. In this table $d_i$ is the average distance between values in the $i$-th estimator.

### 3.30. Artificial Network Fuzzy Inference System (D30)

ANFIS models combine the learning hability of ANNs with the flexibility of fuzzy inference models [51]. They tipically include five layers. The first one

18

Table 11: GRNN optimal configuration.

| Parameter | Value |
|-----------|-------|
| Inputs | $D(0), G(0), R(\theta_{zp}), \theta_{sp}$ |
| Outputs | $D(\theta_{zp}, \gamma_p)$ |
| Bias | $0.9\max(d_i)$ |

contains fixed nodes that define the membership functions to the fuzzy sets. The second layer contains as many adaptative nodes as inference rules. Commonly, they are defined as many inference rules as fuzzy sets. The third layer normalizes the outputs of the previous layer. Next layer includes two fixed nodes which inputs are the normalized outputs of the third layer and the initial inputs. Finally, the last layer defuzzyfies the model outputs.

Including fuzzy sets in ANNs allows the network to behave more smoothly than those which use classical transfer functions. In the particular case of ANFIS, the Sugeno-Tsukamoto fuzzy inference model is applied [102]. Finally, ANFIS training process is carried out in two steps. The first one is a feedforward process where the membership functions parameters are inicialized. The second one consists in the backpropagation of the obtained error from the output of the model.

Table 12: ANFIS optimal configuration.

| Parameter | Value |
|-----------|-------|
| Inputs | $D(0), G(0), R(\theta_{zp}), \theta_{sp}$ |
| Outputs | $D(\theta_{zp}, \gamma_p)$ |
| Fuzzy sets | $\Omega_{i,1}$: low, $\Omega_{i,2}$: mid, $\Omega_{i,3}$: high |
| Membership function | Generalized bell |
| Rules | $4^3 = 64$ |
| Epochs | 42 |

To obtain the optimal configuration of the ANFIS model for the case study, which can be seen in Table 12, first a preliminar analyis of the model with just one epoch, three fuzzy sets for each variable and $n^m$ rules is carried out ($n$ is the number of variables and $m$ the number of fuzzy sets). Then, the RMSD value for the training and checking datasets is compared for the $C_n^k$ candidate models with $n$ candidate input parameters and $k \in \{1, 2, 3, 4\}$ model inputs. Finally, the optimal number of epochs is selected by comparing results from 1 to 100 epochs (see Figure 6).
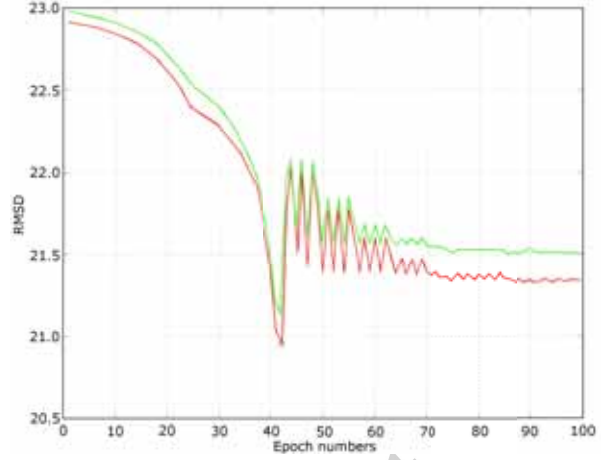


Figure 6: ANFIS training (green) and checking (red) error curves.

## 4. Results and discussion

Tables 13, 14, 15 and 16 show the results for the statistic estimators for the 30 evaluated models with data measured on North, South, East and West directions respectively.

Taylor diagrams with the models results for the same directions are presented in Figures 7, 8, 9 and 10. Taylor diagrams allow the graphical intercomparison of the centered RMSD ($RMSD_c$), the standard deviation and the coefficient of correlation $R$, which is the squared root of the coefficient of determination $R^2$, through a geometrical relation [46]. Let's notice that the centered RMSD is related to the RMSD and MBD statistics through expression (108).

$$RMSD_c^2 = RMSD^2 + MBD^2. \qquad (108)$$

Reference values (black circles on graphs) are the measured data set, which has a known standard deviation and null values of RMSD and $R^2$. On the other hand, *"Three components"* refers to the test data obtained by substraying the direct beam irradiance and the albedo's irradiance from the global tilted measured irradiance (the closer the model icon in the graph to the reference, the better).

It can be shown that most models have a similar correlation coefficient to the reference data. Only 5 models (North) , 2 models (South), 12 models (East) and 4 models (West) show a correlation coefficient less than 0.8. The centered RMSD represented in the graphs shows low values for most models but D06 (ASHRAE) and D07 (Díez-Mediavilla). On the other hand, D27

19

Table 13: Transposition models results and ranking positions for the North direction.

| ID | MBD [W·m$^{-2}$] | RMSD [W·m$^{-2}$] | R$^2$ [-] | t [-] | d [W·m$^{-2}$] | $\mu_{0.99}$ [W·m$^{-2}$] |
|---|---|---|---|---|---|---|
| Isotropic models | | | | | | |
| D01 | −15.2 | 33.6 | 0.74 | 40.5 | 0.91 | −16.0 |
| D02 | −15.2 | 33.6 | 0.74 | 40.5 | 0.91 | −16.0 |
| D03 | −15.2 | 33.6 | 0.74 | 40.5 | 0.91 | −16.0 |
| D04 | 12.3 | 40.1 | 0.71 | 25.8 | 0.90 | +13.4 |
| D05 | 19.3 | 33.0 | 0.79 | 57.4 | 0.90 | +20.0 |
| Anisotropic models | | | | | | |
| D06 | 77.0 | 117.9 | 0.59 | 69.0 | 0.56 | +79.6 |
| D07 | −45.8 | 83.5 | 0.08 | 52.4 | 0.42 | −47.8 |
| D08 | −6.9 | 32.6 | 0.73 | 17.4 | 0.92 | −7.8 |
| D09 | 8.3 | 53.4 | 0.75 | 12.6 | 0.87 | +9.8 |
| D10 | −14.2 | 29.9 | 0.80 | 43.4 | 0.93 | −15.0 |
| D11 | −7.2 | 30.4 | 0.79 | 19.6 | 0.93 | −8.1 |
| D12 | −50.2 | 65.3 | 0.53 | 96.3 | 0.40 | −51.5 |
| D13 | −19.0 | 39.0 | 0.67 | 44.8 | 0.87 | −20.0 |
| D14 | −33.4 | 44.1 | 0.78 | 93.1 | 0.80 | −34.3 |
| D15 | −4.5 | 20.5 | 0.88 | 18.2 | 0.97 | −5.1 |
| D16 | −24.7 | 48.5 | 0.51 | 47.3 | 0.78 | −25.9 |
| D17 | −40.8 | 52.6 | 0.68 | 98.2 | 0.71 | −41.8 |
| D18 | −65.1 | 73.3 | 0.84 | 155 | 0.27 | −66.1 |
| D19 | 10.6 | 40.6 | 0.66 | 21.6 | 0.89 | +11.8 |
| D20 | −35.3 | 61.6 | 0.33 | 56.1 | 0.64 | −36.8 |
| D21 | −39.0 | 51.3 | 0.72 | 93.6 | 0.69 | −40.0 |
| D22 | −20.8 | 34.7 | 0.77 | 59.8 | 0.89 | −21.6 |
| D23 | −14.4 | 33.4 | 0.74 | 38.3 | 0.91 | −15.3 |
| D24 | −36.1 | 48.0 | 0.74 | 91.7 | 0.74 | −37.0 |
| D25 | −32.3 | 42.9 | 0.77 | 91.8 | 0.82 | −33.1 |
| D26 | −58.2 | 67.3 | 0.77 | 138 | 0.42 | −59.2 |
| Non-parametric models | | | | | | |
| D27 | 2.6 | 17.7 | 0.91 | 12.1 | 0.97 | +3.2 |
| D28 | 0.4 | 20.3 | 0.88 | 1.5 | 0.97 | +1.0 |
| D29 | −0.01 | 26.6 | 0.80 | 0.03 | 0.95 | −0.8 |
| D30 | 0.4 | 19.8 | 0.88 | 1.5 | 0.97 | +0.9 |

(Multi-Layer Perceptron) shows the best performance for all directions, with extraordinary good results for the South. In general terms, non-parametrical models show better results in all cases than parametrical ones. Isotropic models behave quite good for all directions but the North. D14 and D15 (Perez et al.), D16 (Reindl) and D18 (Steven & Unsworth) show the best performances from the anisotropic group.

Table 17 shows the statistical significance calculation for each model group benchmark. This non-parametric statistical procedure for ranking the overall performance of models was originally presented by Stone for models results on different locations [44]. In this case, it has been adapted to data from one location but several directions of measurement. $L$ statistic is defined in [44] as a statistic of agreement which measures the success of the alternative hypothesis in two respects. Firstly, it reflects success in predicting the order of the sample sum of ranks. Secondly, it represents the tendency of the sum

of the ranks to be widely separated. $E(L)$ is the expected value of $L$, $Var(L)$ is the variance of $L$, $z$ is the conversion of the $L$ statistic to a standard score of the normal distribution and, finally, $\alpha$ is the statistical significance of the aggregation or global rank. Results for each parameter have been calculated for each model class and for the complete selection of models.

Figures 11, 12 and 13 show the results of the benchmarking for the MBD, RMSD and $\mu_{0.99}$ statistical estimators respectively. These graphs expose, including a colourful scale, the position differences in the aggregated ranking between the models in the horizontal axis respect the vertical axis. A positive value $x_{AB}$ indicates that model $A$, in the horizontal axis, is placed $x$ positions lower in the ranking with respect to the model $B$, in the vertical axis. This means that model $A$ would behave worse than model $B$, according to the considered statistical estimator. A negative value of $x_{AB}$ would mean the opposite. The greater the $x$ value, the major the dif-

20

Table 14: Transposition models results and ranking positions for the South direction.

| ID | MBD [W·m⁻²] | RMSD [W·m⁻²] | $R^2$ [-] | t [-] | d [W·m⁻²] | $\mu_{0.99}$ [W·m⁻²] |
|---|---|---|---|---|---|---|
| | | | Isotropic models | | | |
| D01 | −42.6 | 67.3 | 0.75 | 65.5 | 0.78 | −44.1 |
| D02 | −42.6 | 67.3 | 0.75 | 65.5 | 0.78 | −44.1 |
| D03 | −42.6 | 67.3 | 0.75 | 65.5 | 0.78 | −44.1 |
| D04 | −15.1 | 50.0 | 0.74 | 25.4 | 0.90 | −16.5 |
| D05 | 52.6 | 85.7 | 0.66 | 62.2 | 0.82 | +54.5 |
| | | | Anisotropic models | | | |
| D06 | 120 | 158.8 | 0.68 | 91.9 | 0.60 | +122.8 |
| D07 | −73.2 | 109.6 | 0.24 | 71.9 | 0.38 | −75.6 |
| D08 | 35.8 | 62.2 | 0.75 | 56.5 | 0.89 | +37.3 |
| D09 | −4.0 | 65.7 | 0.67 | 4.9 | 0.89 | −6.0 |
| D10 | −41.7 | 67.4 | 0.74 | 63.0 | 0.78 | −43.2 |
| D11 | −28.1 | 48.2 | 0.85 | 57.4 | 0.91 | −29.2 |
| D12 | −32.8 | 55.0 | 0.81 | 59.4 | 0.87 | −34.1 |
| D13 | −22.4 | 44.8 | 0.83 | 46.3 | 0.93 | −23.5 |
| D14 | −19.5 | 40.7 | 0.86 | 43.6 | 0.94 | −20.5 |
| D15 | −5.6 | 32.4 | 0.88 | 14.1 | 0.97 | −6.5 |
| D16 | −15.6 | 38.3 | 0.86 | 35.7 | 0.95 | −16.6 |
| D17 | −44.1 | 62.0 | 0.80 | 81.2 | 0.84 | −45.4 |
| D18 | 25.4 | 64.3 | 0.60 | 34.3 | 0.85 | +27.1 |
| D19 | 14.9 | 49.4 | 0.74 | 25.3 | 0.91 | +16.2 |
| D20 | −11.6 | 58.1 | 0.65 | 16.3 | 0.89 | −13.2 |
| D21 | 7.3 | 49.4 | 0.73 | 11.9 | 0.90 | +8.7 |
| D22 | −15.9 | 37.9 | 0.86 | 37.1 | 0.95 | −16.9 |
| D23 | −40.7 | 65.8 | 0.76 | 63.1 | 0.79 | −42.2 |
| D24 | −19.8 | 41.0 | 0.85 | 44.1 | 0.95 | −20.9 |
| D25 | −59.7 | 82.5 | 0.76 | 84.1 | 0.63 | −61.4 |
| D26 | 28.6 | 56.7 | 0.74 | 46.9 | 0.90 | +30.0 |
| | | | Non-parametric models | | | |
| D27 | 0.2 | 7.7 | 0.99 | 2.6 | 1.00 | +0.5 |
| D28 | 0.3 | 36.0 | 0.85 | 0.6 | 0.96 | +1.3 |
| D29 | −0.4 | 47.9 | 0.75 | 0.6 | 0.93 | −1.8 |
| D30 | 0.2 | 29.5 | 0.90 | 0.5 | 0.97 | +1.0 |

ference in ranking positions and model's performance. Notice that isotropic models D01 (Liu & Jordan), D02 (Tian et al.) and D03 (Badescu) have the same ranking positions because their expressions for vertical surfaces become strictly the same.

Overall behaviour of benchmarks is found to be similar according to the three considered statistical estimators, but certain ranking position differences can be found.

For the North direction, it can be seen that most models have a good performance. Apart from models D06 and D07, RMSD value is always less than 80 W·m⁻², and apart from models D06, D07, D12, D13, D16, D17, D19 and D20 the coefficient of determination $R^2$ is in the range $(0.70, 0.96)$. Not important differences between isotropic and anisotropic models can be observed in this case. According to Table 13, isotropic models (3 out of 5) and most anisotropic ones (18 out of 21, except D06, D09 and D19) tend to underestimate the

diffuse irradiance. On the other hand, non-parametric models, except D29 (GRNN), tend to overestimate always the irradiance value. Nevertheless, D29 model obtains the best results for the MBD, $t$-statistic and $\mu_{0.99}$ estimators. From a global point of view, isotropic models behave the best for the North direction in the case study, specially D04 (Koronakis) and D05 (Olmo) models. Finally, focusing on the anisotropic models, major differences between them can be observed rather than between the isotropic ones. From this classification, D15 (locally optimized Perez et al.) model behaves extremely well, far away from the same model with general coefficients (D14). Moreover, no significant differences between anisotropic by superposition and anisotropic by gradient models can be found.

If we observe the South direction results, its associated Taylor Diagram has a quite similar shape than the one obtained for the North direction. In this case, all models, except D07, have a correlation coefficient

21

Table 15: Transposition models results and ranking positions for the East direction.

| ID | MBD [W·m$^{-2}$] | RMSD [W·m$^{-2}$] | R$^2$ [-] | t [-] | d [W·m$^{-2}$] | $\mu_{0.99}$ [W·m$^{-2}$] |
|---|---|---|---|---|---|---|
| **Isotropic models** | | | | | | |
| D01 | −42.9 | 73.2 | 0.48 | 58.0 | 0.68 | −44.7 |
| D02 | −42.9 | 73.2 | 0.48 | 58.0 | 0.68 | −44.7 |
| D03 | −42.9 | 73.2 | 0.48 | 58.0 | 0.68 | −44.7 |
| D04 | −15.4 | 64.1 | 0.46 | 19.8 | 0.80 | −17.2 |
| D05 | 1.7 | 66.4 | 0.43 | 2.0 | 0.80 | +3.6 |
| **Anisotropic models** | | | | | | |
| D06 | 74.3 | 122 | 0.46 | 61.4 | 0.64 | +77.1 |
| D07 | −73.5 | 115 | 0.06 | 66.8 | 0.18 | −76.1 |
| D08 | −9.6 | 49.6 | 0.65 | 15.8 | 0.89 | −11.0 |
| D09 | −11.3 | 57.9 | 0.69 | 15.9 | 0.89 | −13.0 |
| D10 | −42.0 | 71.5 | 0.51 | 58.2 | 0.70 | −43.7 |
| D11 | −31.5 | 58.4 | 0.64 | 51.2 | 0.83 | −32.9 |
| D12 | −60.6 | 81.1 | 0.66 | 90.0 | 0.55 | −62.2 |
| D13 | −33.4 | 54.1 | 0.75 | 62.7 | 0.85 | −34.6 |
| D14 | −41.5 | 56.1 | 0.85 | 88.2 | 0.83 | −42.6 |
| D15 | −4.4 | 29.6 | 0.87 | 12.1 | 0.97 | −5.3 |
| D16 | −30.2 | 52.2 | 0.74 | 56.7 | 0.86 | −31.4 |
| D17 | −55.1 | 70.0 | 0.79 | 102.1 | 0.72 | −56.3 |
| D18 | −40.3 | 76.1 | 0.42 | 50.1 | 0.71 | −42.2 |
| D19 | −5.5 | 55.4 | 0.56 | 7.9 | 0.85 | −7.1 |
| D20 | −24.0 | 79.2 | 0.38 | 25.5 | 0.75 | −26.2 |
| D21 | −32.1 | 58.3 | 0.68 | 52.9 | 0.81 | −33.6 |
| D22 | −29.0 | 50.7 | 0.75 | 55.8 | 0.88 | −30.2 |
| D23 | −41.6 | 72.2 | 0.49 | 56.4 | 0.69 | −43.3 |
| D24 | −40.4 | 53.4 | 0.85 | 92.5 | 0.86 | −41.4 |
| D25 | −60.1 | 84.4 | 0.50 | 81.0 | 0.52 | −61.8 |
| D26 | −31.1 | 57.1 | 0.66 | 51.9 | 0.85 | −32.5 |
| **Non-parametric models** | | | | | | |
| D27 | 0.9 | 10.4 | 0.98 | 7.1 | 1.00 | +1.2 |
| D28 | 0.9 | 31.1 | 0.86 | 2.4 | 0.96 | +1.8 |
| D29 | −0.3 | 58.2 | 0.56 | 0.4 | 0.86 | −2.0 |
| D30 | 0.8 | 29.1 | 0.87 | 2.2 | 0.97 | +1.6 |

greater than 0.80, and the RMSD value is close to 50 W·m$^{-2}$ for most models. Except model D06, obtained standard deviations are in the range (48, 130) W·m$^{-2}$. It also can be observed that D09 and D05 models behave surprisingly similar and the non-parametric model D27 offers extremely good estimations. Taking into account the sign of the $\mu_{0.99}$ statistical estimator, most models tend to underestimate the diffuse irradiance for the South direction. Furthermore, it can be observed again that non-parametric models behave the best. On the other hand, in this case significant differences between anisotropic models and isotropic ones have been detected. The best parametric models in this case are D15 and D09 according to MBD and $\mu_{0.99}$ statistics. However, the reader must be awarded that model D09 has a low value for the determination coefficient $R^2$. Best anisotropic by gradient models are D21 (Brunger & Hooper) and D24 (Iwaga et al.) respectively. For this direction, D04 model is the best isotropic one.

For the East direction case study, the Taylor Diagram shows major dispersion on the results than the previous cases. The average correlation coefficient decreases, but the RMSD results do not increase significantly. It can be observed again that D27 model obtains the best results. D28 (RBF), D29, D30 (ANFIS), D15, D24, D21 and D17 (Skartveit & Olseth) also show good results. D06 model shows the highest value for the RMSD estimator. On the other hand, a higher average value for RMSD for isotropic models can be observed. Furthermore, results on Table 15 show that models D06, D27, D28 and D30 tend to underestimate. Model D27 shows the best results for the RMSD, $R^2$, $d$ and $\mu_{0.99}$ statistical estimators, but model D29 performs better according to MBD and $t$-statistic. D05 shows the best performance from the isotropic models group. However, it has been observed that this model has a significantly low value of the correlation coefficient. Finally, for this cardinal direction, the best anisotropic models are D15, D19, D22

22

Table 16: Transposition models results and ranking positions for the West direction.

| ID | MBD [W·m$^{-2}$] | RMSD [W·m$^{-2}$] | R$^2$ [-] | t [-] | d [W·m$^{-2}$] | $\mu_{0.99}$ [W·m$^{-2}$] |
|---|---|---|---|---|---|---|
| | | | Isotropic models | | | |
| D01 | −21.4 | 41.8 | 0.73 | 47.9 | 0.88 | −22.5 |
| D02 | −21.4 | 41.8 | 0.73 | 47.9 | 0.88 | −22.5 |
| D03 | −21.4 | 41.8 | 0.73 | 47.9 | 0.88 | −22.5 |
| D04 | 6.0 | 39.0 | 0.72 | 12.5 | 0.92 | +7.2 |
| D05 | 30.8 | 50.1 | 0.68 | 62.3 | 0.85 | +31.9 |
| | | | Anisotropic models | | | |
| D06 | 88.2 | 123.1 | 0.70 | 82.3 | 0.61 | +90.7 |
| D07 | −52.0 | 84.5 | 0.21 | 62.5 | 0.48 | −54.0 |
| D08 | 4.3 | 35.1 | 0.77 | 9.9 | 0.93 | +5.3 |
| D09 | 4.1 | 60.7 | 0.62 | 5.5 | 0.85 | +5.9 |
| D10 | −20.5 | 41.2 | 0.73 | 46.0 | 0.88 | −21.6 |
| D11 | −12.7 | 35.8 | 0.77 | 30.4 | 0.92 | −13.7 |
| D12 | −45.4 | 61.5 | 0.69 | 87.6 | 0.67 | −46.6 |
| D13 | −21.7 | 39.5 | 0.77 | 52.7 | 0.90 | −22.7 |
| D14 | −29.9 | 42.6 | 0.83 | 78.8 | 0.87 | −30.7 |
| D15 | −6.7 | 26.5 | 0.86 | 20.9 | 0.96 | −7.4 |
| D16 | −25.3 | 44.6 | 0.71 | 55.0 | 0.87 | −26.3 |
| D17 | −43.5 | 55.5 | 0.78 | 101 | 0.76 | −44.5 |
| D18 | −34.1 | 72.9 | 0.32 | 42.4 | 0.68 | −36.0 |
| D19 | 12.0 | 38.3 | 0.74 | 26.5 | 0.92 | +13.1 |
| D20 | −34.5 | 56.3 | 0.59 | 62.2 | 0.78 | −35.8 |
| D21 | −21.0 | 43.4 | 0.70 | 44.5 | 0.87 | −22.2 |
| D22 | −15.7 | 32.2 | 0.83 | 44.9 | 0.94 | −16.6 |
| D23 | −20.2 | 41.0 | 0.73 | 45.3 | 0.89 | −21.2 |
| D24 | −29.6 | 41.7 | 0.82 | 80.4 | 0.89 | −30.4 |
| D25 | −38.6 | 53.8 | 0.74 | 82.5 | 0.77 | −39.7 |
| D26 | −22.2 | 48.1 | 0.65 | 41.7 | 0.87 | −23.4 |
| | | | Non-parametric models | | | |
| D27 | 0.002 | 5.2 | 0.99 | 0.0 | 1.00 | +0.1 |
| D28 | 0.06 | 26.7 | 0.85 | 0.2 | 0.96 | +0.8 |
| D29 | −0.7 | 42.9 | 0.64 | 1.3 | 0.89 | −1.9 |
| D30 | 0.2 | 24.6 | 0.87 | 0.7 | 0.96 | +0.9 |

Table 17: Statistical values from the non-parametric aggregation.

| Models | L | E(L) | Var(L) | z | α |
|---|---|---|---|---|---|
| | | MBD | | | |
| Isotropic | 166 | 180 | 100 | −1.400 | 0.075 |
| Anisotropic | 12 765 | 10 164 | 118 580 | 7.553 | 0.000 |
| Non-param. | 103 | 100 | 33.333 | 0.520 | 0.174 |
| All | 36 513 | 28 830 | 696 725 | 9.204 | 0.000 |
| | | RMSD | | | |
| Isotropic | 159 | 180 | 100 | −2.100 | 0.022 |
| Anisotropic | 12 795 | 10 164 | 118 580 | 7.640 | 0.000 |
| Non-param. | 116 | 100 | 33.333 | 2.771 | 0.004 |
| All | 36 074 | 28 830 | 696 725 | 8.679 | 0.000 |
| | | $\mu_{0.99}$ | | | |
| Isotropic | 166 | 180 | 100 | −1.400 | 0.075 |
| Anisotropic | 12 792 | 10 164 | 118 580 | 7.632 | 0.000 |
| Non-param. | 110 | 100 | 33.333 | 1.732 | 0.044 |
| All | 36 470 | 28 830 | 696 725 | 9.153 | 0.000 |

(CIE 2004) and D26 (Siala & Hooper). Nevertheless, no significant differences are observed between anisotropic by superposition and anisotropic by gradient models in this case.

On the other hand, Figures 11, 12 and 13 show the benchmark matrix for the non-parametric aggregation for the four cardinal directions and for the MBD, RMSD and $\mu_{0.99}$ statistical estimators, respectively. The three graphs show a similar behaviour in the colour scale. In all cases several clusters can be observed, highlighting the non-parametrical models (up right corner) and the isotropic ones (low left corner). Differences between models are much more highlighted in the RMSD benchmark graph than the one for the MBD. Although this tool helps to compare models performances by pairs, benchmark positions for anisotropic models change as function of the considered statistical estimator.

According to previous models intercomparison studies, obtained results are coherent with them, although

very few studies compare 10-min. averaged data on several azimuth angles.

Let's notice that previous studies, such as [60, 103] highlight the fact that the correct modeling of the reflected irradiance, as well as the experimental apparatus, are of key importance when dealing with off-south surfaces because the reflectance of a natural surface is never perfectly isotropic. This may not affect significantly south-facing tilting surfaces because the sky diffuse is relatively large for this direction. However, for other vertical orientations, errors in the calculated reflected irradiance can be relatively significant, thus yielding errors of opposite sign in the observed tilted diffuse that is taken as the reference, but which is generally calculated as the difference between the total tilted diffuse and the reflected irradiance. This can be avoided adding a mask or shield to the sensor to block the reflected irradiance, but this cannot be perfect either.

On the other hand, current solar radiation models and measures are rather comparable because of the absolute measurement uncertainties [104, 105]. In many cases, these uncertainties are of higher value than the

models bias errors. Thus, the challenge for solar radiation misprints and models is to reduce the uncertainty in measured data, as well as develop more robust models with fewer input parameters and smaller residuals, under a wider variety of conditions [105]. In this case, where measured diffuse irradiances were in the range [0, 350] W·m$^{-2}$, absolute uncertainties result always smaller than 20 W·m$^{-2}$ (let's also notice that maximum relative uncertainty is obtained for low values of measured irradiance and it decreases as the measured value increases) and, thus, observed differences on some models, specially according to MBD estimator, may be neglected, e.g. non-parametric models. This observation must be taken into account in order not to incur in erroneous conclusions.

There exist many studies that compare radiation models, specially with measurements on tilted surfaces to the South direction. It is also common to use hourly, daily or monthly averaged values which reduce the relative uncertainty. Nevertheless, found results in our work are coherent with those obtained in [34, 56, 106, 107, 108], where also find slight differences between ana-
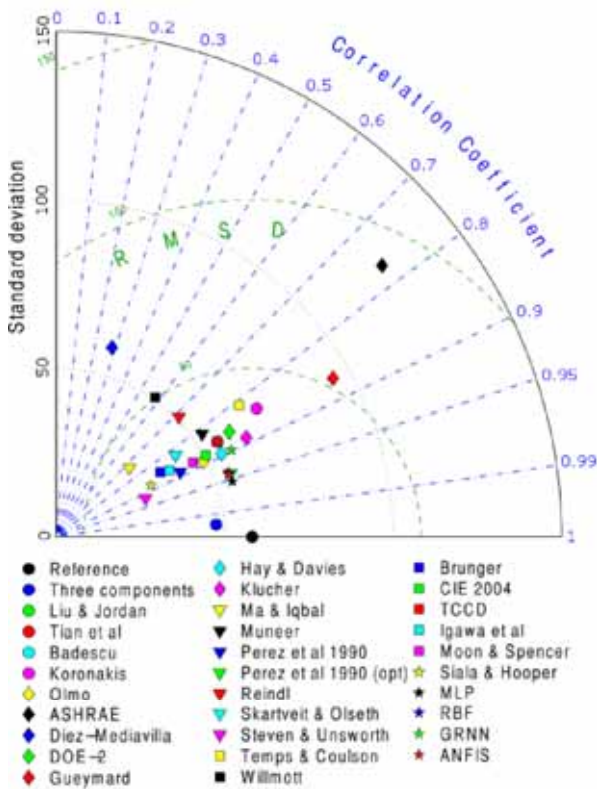


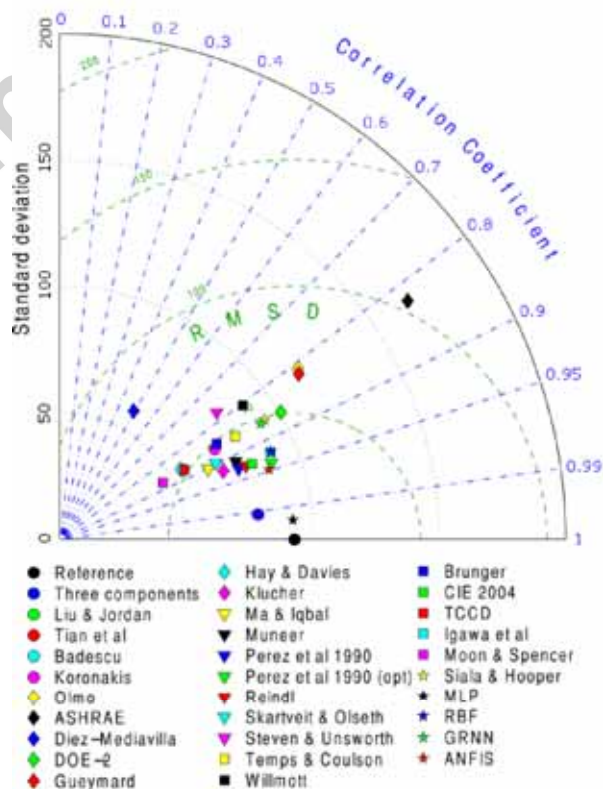Figure 7: Taylor diagram for North direction estimations.



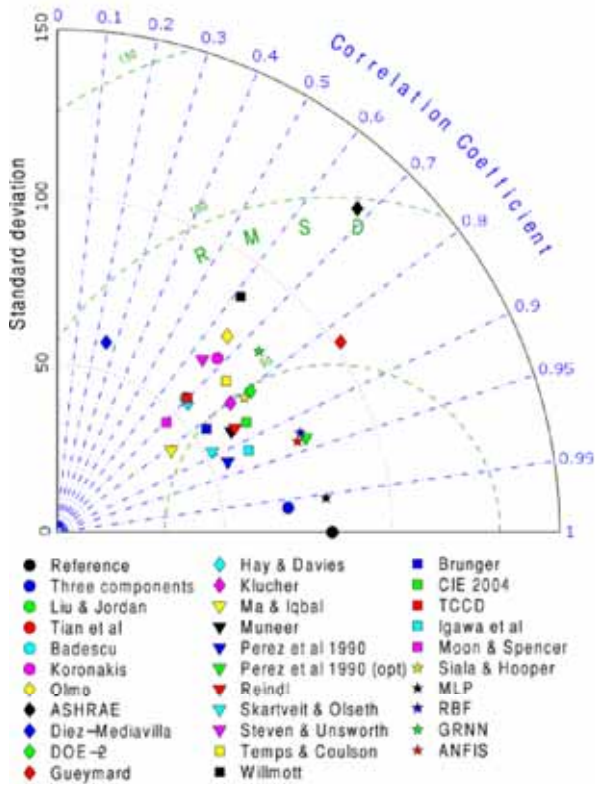Figure 8: Taylor diagram for South direction estimations.

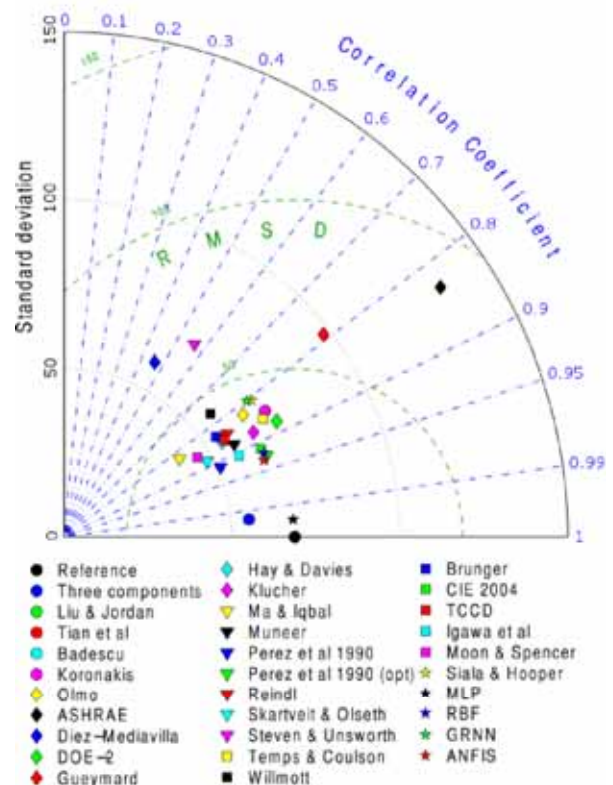Figure 9: Taylor diagram for East direction estimations.



Figure 10: Taylor diagram for West direction estimations.

lyzed models and the MBD and RMSD values are in a similar range than in this work. Morever, these studies also rank Perez et al. model in the top and Koronakis model have the best performance for isotropy conditions under intermediate and overcast skies. Higher discrepancies can be found related to the Skartveit & Olseth and the Steven & Unsworth models, that are ranked in better positions than in our study. Also, studies which evaluate transposition models on different azimuth angles find worse results for East and West directions rather than on the South one [106, 107].

Studies about non-parametric models [83, 109] also conclude that this group of models have better accuracy and a more realistic performance than the parametric models group. However, [83] finds better performance on GRNN models than on MLP models although this one offers a better determination coefficient value on the test.

One of the latest studies in this field is [87]. Although it includes an extensive review of transposition models (only isotropic and anisotropic by superposition models) and correct some errors in the literature some dis-

crepances are found with our work. Major discrepancies are found on the interpretation of the Olmo's model and the circumsolar anisotropy in Steven & Unsworth model. Nevertheless we agree with no universal model can be concluded. The author also finds Perez et al.'s one of the best models.

Finally, major differences have been found with [86, 110] because of the significantly different climatic conditions and the reduced dataset used in the second case.

## 5. Conclusions

As result of the carried out review, four main model classes can be distinguished: isotropic models, anisotropic superposition models, relative radiance anisotropic models and non-parametric models.

According to the results, differences on the models performances for several directions were found. The most accurate estimations for the case study and the aggregation of the four directions have been obtained by the non-parametric models. From these, the Multi-Layer Perceptron (MLP) obtained the best results

but uncertainties on the measurement made all non-parametric models estimations almost indistinguishable (as differences were lower than the measurement uncertainties). From the parametric models, the one which estimations were closest to the reference dataset was the Perez et al. model with local fitted coefficients. Original Perez et al., Reindl and Igawa et al. models also performed well. On the other hand, the ASHRAE and Díez-Mediavilla models performed the worst in most cases and they may be selected with caution for high accuracy modelling.

The benchmark analysis for all directions and sky conditions allowed clustering the best and worst models. For the three statistical estimators MBD, RMSD and $\mu_{0.99}$, best models are found to be the non-parametric models (MLP, RBF, GRNN and ANFIS), CIE2004, Temps & Coulson, Perez et al. locally fitted coefficients and Koronakis. On the other hand, the worst results have been obtained by ASHRAE, Díez-Mediavilla, Ma & Iqbal, Skartveit & Olseth, Steven & Unsworth, Moon & Spencer and Siala & Hooper. Differences in the aggregated rank possitions have been found intensified for the RMSD estimator.

If single directions are considered, apart from the non-parametric models that achieve the best results in all cases, the optimized Perez et al. model has the best results for the statistical estimators for the North direction but the $t$-statistics, which lowest value has been obtained by the Gueymard model. For this direction, according to the MBD sign, most models tend to underestimate diffuse irradiance (22 out of 30). For the South direction, optimized Perez et al. model obtains again the best results for all statistical estimators but the MBD and the $\mu_{0.99}$ which were achieved for the Gueymard model. In this case, 20 models out of 30 tend to underestimate the diffuse irradiance value. For the East and West directions, optimized Perez et al. model performs the best according to the RMSD and $R^2$ values. However, for the East direction, the Olmo model performs better for the MBD and $\mu_{0.99}$ estimators, and the Temps & Coulson model obtains the best result for the $t$-statistic. On the other hand, for the West direction, the Gueymard model obtains the best value of the MBD, but the DOE-2 model performs better according to the Willmott's $d$ and the $\mu_{0.99}$ estimators. Moon & Spencer and Brunger & Hooper models tend to underestimate the measured diffuse irradiance for the East and West directions, respectively.

Finally, models tendencies to underestimate or overestimate remain for all directions with the exception of the Koronakis, Díez-Mediavilla, DOE-2, Hay & Davies, Steven & Unsworth, Brunger & Hooper and Siala &

Hooper models. According to the proposed classification, the isotropic and relative radiance anisotropic models tend to underestimate, but the non-parametric models tend to overestimate for all studied directions.

Future development of solar radiation models will be linked to increase accuracy when the reduction on the uncertainty in measured data would be feasible and future trends will lead to develop simpler models with fewer input parameters and good performance under all-sky wheather conditions.

## Appendix A. Notes on the nomenclature

To unify nomenclature about irradiance, the following criteria have been applied. The general expression is in the form: $A(\theta_z, \gamma)$, where $A$ is the irradiance component ($B$: direct beam, $D$: diffuse or $R$: reflected) and terms in brakets refer to the zenith angle and azimuth angle of the measurement, respectively. In case the value is referred to a normal plane to the direct beam irradiance, it is expressed with $n$ in brackets. However, when the value is referred to the horizontal plane ($\theta_z = 0$), it results independent from the azimuth angle. Thus, only 0 is indicated in brackets. For the reflectance irradiance in an horizontal surface opposite to the ground, 180 is indicated instead.

## References

[1] Z. Sen, Solar energy in progress and future research trends, Progress in Energy and Combustion Science 30 (4) (2004) 367–416.

[2] A. Strzalka, N. Alam, E. Duminil, V. Coors, U. Eicker, Large scale integration of photovoltaics in cities, Applied Energy 93 (2012) 413–421. doi:10.1016/j.apenergy.2011.12.033.

[3] H. Bunyan, W. Ali, Performance evaluation of photovoltaic module at different tilt angle in kuwait, in: 2014 International Conference and Utility Exhibition on Green Energy for Sustainable Development (ICUE), 2014, pp. 1–4.

[4] E. Roohollahi, M. A. Mehrabian, M. Abdolzadeh, Prediction of solar energy gain on 3-D geometries, Energy and Buildings 62 (2013) 315–322. doi:10.1016/j.enbuild.2013.03.008.

[5] M. De Carli, M. Tonon, Effect of modelling solar radiation on the cooling performance of radiant floors, Solar Energy 85 (5) (2011) 689–712.

| | D01 | D02 | D03 | D04 | D05 | D06 | D07 | D08 | D09 | D10 | D11 | D12 | D13 | D14 | D15 | D16 | D17 | D18 | D19 | D20 | D21 | D22 | D23 | D24 | D25 | D26 | D27 | D28 | D29 | D30 |
|---|---|---|---|---|---|---|---|---|---|---|---|---|---|---|---|---|---|---|---|---|---|---|---|---|---|---|---|---|---|---|
| D30 | 14 | 14 | 14 | 6 | 13 | 22 | 21 | 7 | 4 | 13 | 8 | 19 | 12 | 15 | 3 | 11 | 20 | 17 | 5 | 12 | 10 | 9 | 12 | 15 | 18 | 16 | 1 | 2 | 1 | 0 |
| D29 | 13 | 13 | 13 | 5 | 12 | 21 | 20 | 6 | 3 | 12 | 7 | 18 | 11 | 14 | 2 | 10 | 19 | 16 | 4 | 11 | 9 | 8 | 11 | 14 | 17 | 15 | 0 | 1 | 0 | -1 |
| D28 | 12 | 12 | 12 | 4 | 11 | 20 | 19 | 5 | 2 | 11 | 6 | 17 | 10 | 13 | 1 | 9 | 18 | 15 | 3 | 10 | 8 | 7 | 10 | 13 | 16 | 14 | -1 | 0 | -1 | -2 |
| D27 | 13 | 13 | 13 | 5 | 12 | 21 | 20 | 6 | 3 | 12 | 7 | 18 | 11 | 14 | 2 | 10 | 19 | 16 | 4 | 11 | 9 | 8 | 11 | 14 | 17 | 15 | 0 | 1 | 0 | -1 |
| D26 | -2 | -2 | -2 | -10 | -3 | 6 | 5 | -9 | -12 | -3 | -8 | 3 | -4 | -1 | -13 | -5 | 4 | 1 | -11 | -4 | -6 | -7 | -4 | -1 | 2 | 0 | -15 | -14 | -15 | -16 |
| D25 | -4 | -4 | -4 | -12 | -5 | 4 | 3 | -11 | -14 | -5 | -10 | 1 | -6 | -3 | -15 | -7 | 2 | -1 | -13 | -6 | -8 | -9 | -6 | -3 | 0 | -2 | -17 | -16 | -17 | -18 |
| D24 | -1 | -1 | -1 | -9 | -2 | 7 | 6 | -8 | -11 | -2 | -7 | 4 | -3 | 0 | -12 | -4 | 5 | 2 | -10 | -3 | -5 | -6 | -3 | 0 | 3 | 1 | -14 | -13 | -14 | -15 |
| D23 | 2 | 2 | 2 | -6 | 1 | 10 | 9 | -5 | -8 | 1 | -4 | 7 | 0 | 3 | -9 | -1 | 8 | 5 | -7 | 0 | -2 | -3 | 0 | 3 | 6 | 4 | -11 | -10 | -11 | -12 |
| D22 | 5 | 5 | 5 | -3 | 4 | 13 | 12 | -2 | -5 | 4 | -1 | 10 | 3 | 6 | -6 | 2 | 11 | 8 | -4 | 3 | 1 | 0 | 3 | 6 | 9 | 7 | -8 | -7 | -8 | -9 |
| D21 | 4 | 4 | 4 | -4 | 3 | 12 | 11 | -3 | -6 | 3 | -2 | 9 | 2 | 5 | -7 | 1 | 10 | 7 | -5 | 2 | 0 | -1 | 2 | 5 | 8 | 6 | -9 | -8 | -9 | -10 |
| D20 | 2 | 2 | 2 | -6 | 1 | 10 | 9 | -5 | -8 | 1 | -4 | 7 | 0 | 3 | -9 | -1 | 8 | 5 | -7 | 0 | -2 | -3 | 0 | 3 | 6 | 4 | -11 | -10 | -11 | -12 |
| D19 | 9 | 9 | 9 | 1 | 8 | 17 | 16 | 2 | -1 | 8 | 3 | 14 | 7 | 10 | -2 | 6 | 15 | 12 | 0 | 7 | 5 | 4 | 7 | 10 | 13 | 11 | -4 | -3 | -4 | -5 |
| D18 | -3 | -3 | -3 | -11 | -4 | 5 | 4 | -10 | -13 | -4 | -9 | 2 | -5 | -2 | -14 | -6 | 3 | 0 | -12 | -5 | -7 | -8 | -5 | -2 | 1 | -1 | -16 | -15 | -16 | -17 |
| D17 | -6 | -6 | -6 | -14 | -7 | 2 | 1 | -13 | -16 | -7 | -12 | -1 | -8 | -5 | -17 | -9 | 0 | -3 | -15 | -8 | -10 | -11 | -8 | -5 | -2 | -4 | -19 | -18 | -19 | -20 |
| D16 | 3 | 3 | 3 | -5 | 2 | 11 | 10 | -4 | -7 | 2 | -3 | 8 | 1 | 4 | -8 | 0 | 9 | 6 | -6 | 1 | -1 | -2 | 1 | 4 | 7 | 5 | -10 | -9 | -10 | -11 |
| D15 | 11 | 11 | 11 | 3 | 10 | 19 | 18 | 4 | 1 | 10 | 5 | 16 | 9 | 12 | 0 | 8 | 17 | 14 | 2 | 9 | 7 | 6 | 9 | 12 | 15 | 13 | -2 | -1 | -2 | -3 |
| D14 | -1 | -1 | -1 | -9 | -2 | 7 | 6 | -8 | -11 | -2 | -7 | 4 | -3 | 0 | -12 | -4 | 5 | 2 | -10 | -3 | -5 | -6 | -3 | 0 | 3 | 1 | -14 | -13 | -14 | -15 |
| D13 | 2 | 2 | 2 | -6 | 1 | 10 | 9 | -5 | -8 | 1 | -4 | 7 | 0 | 3 | -9 | -1 | 8 | 5 | -7 | 0 | -2 | -3 | 0 | 3 | 6 | 4 | -11 | -10 | -11 | -12 |
| D12 | -5 | -5 | -5 | -13 | -6 | 3 | 2 | -12 | -15 | -6 | -11 | 0 | -7 | -4 | -16 | -8 | 1 | -2 | -14 | -7 | -9 | -10 | -7 | -4 | -1 | -3 | -18 | -17 | -18 | -19 |
| D11 | 6 | 6 | 6 | -2 | 5 | 14 | 13 | -1 | -4 | 5 | 0 | 11 | 4 | 7 | -5 | 3 | 12 | 9 | -3 | 4 | 2 | 1 | 4 | 7 | 10 | 8 | -7 | -6 | -7 | -8 |
| D10 | 1 | 1 | 1 | -7 | 0 | 9 | 8 | -6 | -9 | 0 | -5 | 6 | -1 | 2 | -10 | -2 | 7 | 4 | -8 | -1 | -3 | -4 | -1 | 2 | 5 | 3 | -12 | -11 | -12 | -13 |
| D09 | 10 | 10 | 10 | 2 | 9 | 18 | 17 | 3 | 0 | 9 | 4 | 15 | 8 | 11 | -1 | 7 | 16 | 13 | 1 | 8 | 6 | 5 | 8 | 11 | 14 | 12 | -3 | -2 | -3 | -4 |
| D08 | 7 | 7 | 7 | -1 | 6 | 15 | 14 | 0 | -3 | 6 | 1 | 12 | 5 | 8 | -4 | 4 | 13 | 10 | -2 | 5 | 3 | 2 | 5 | 8 | 11 | 9 | -6 | -5 | -6 | -7 |
| D07 | -7 | -7 | -7 | -15 | -8 | 1 | 0 | -14 | -17 | -8 | -13 | -2 | -9 | -6 | -18 | -10 | -1 | -4 | -16 | -9 | -11 | -12 | -9 | -6 | -3 | -5 | -20 | -19 | -20 | -21 |
| D06 | -8 | -8 | -8 | -16 | -9 | 0 | -1 | -15 | -18 | -9 | -14 | -3 | -10 | -7 | -19 | -11 | -2 | -5 | -17 | -10 | -12 | -13 | -10 | -7 | -4 | -6 | -21 | -20 | -21 | -22 |
| D05 | 1 | 1 | 1 | -7 | 0 | 9 | 8 | -6 | -9 | 0 | -5 | 6 | -1 | 2 | -10 | -2 | 7 | 4 | -8 | -1 | -3 | -4 | -1 | 2 | 5 | 3 | -12 | -11 | -12 | -13 |
| D04 | 8 | 8 | 8 | 0 | 7 | 16 | 15 | 1 | -2 | 7 | 2 | 13 | 6 | 9 | -3 | 5 | 14 | 11 | -1 | 6 | 4 | 3 | 6 | 9 | 12 | 10 | -5 | -4 | -5 | -6 |
| D03 | 0 | 0 | 0 | -8 | -1 | 8 | 7 | -7 | -10 | -1 | -6 | 5 | -2 | 1 | -11 | -3 | 6 | 3 | -9 | -2 | -4 | -5 | -2 | 1 | 4 | 2 | -13 | -12 | -13 | -14 |
| D02 | 0 | 0 | 0 | -8 | -1 | 8 | 7 | -7 | -10 | -1 | -6 | 5 | -2 | 1 | -11 | -3 | 6 | 3 | -9 | -2 | -4 | -5 | -2 | 1 | 4 | 2 | -13 | -12 | -13 | -14 |
| D01 | 0 | 0 | 0 | -8 | -1 | 8 | 7 | -7 | -10 | -1 | -6 | 5 | -2 | 1 | -11 | -3 | 6 | 3 | -9 | -2 | -4 | -5 | -2 | 1 | 4 | 2 | -13 | -12 | -13 | -14 |

Figure 11: Transposition models benchmark for all directions according to MBD.

[6] C. Stanciu, D. Stanciu, Optimum tilt angle for flat plate collectors all over the World – A declination dependence formula and comparisons of three solar radiation models, Energy Conversion and Management 81 (2014) 133–143.

[7] M. de Simón-Martín, M. Díez-Mediavilla, C. Alonso-Tristán, Modelling solar data: reasons, main methods and applications, in: International Conference on Renewable Energies and Power Quality (ICREPQ'13) Proceedings, Vol. 1, European Association for the Development of Renewable Energies, Environment and Power Quality (EA4EPQ), Bilbao (Spain), 2013, pp. 1–5.

[8] C. Demain, M. Journée, C. Bertrand, Evaluation of different models to estimate the global solar radiation on inclined surfaces, Renewable Energy 50 (2013) 710–721.

[9] European Commision, Treaty on European Union (Feb. 1992).

[10] The Johannesburg Renewable Energy Coalition, Communication from the Commission Europe 2020. A strategy for smart, sustainable and inclusive growth (Mar. 2010).

[11] European Commission, Implementing the Energy Performance of Buildings Directive (EPBD). Featuring Country Reports 2012, Electronic version, 2013.

[12] European Commission, Communication from the Commission Europe 2020. A strategy for smart, sustainable and inclusive growth (Mar. 2010).

[13] European Commission, Council Decision 2002/358/CE of 25 April 2002 concerning the approval, on behalf of the European Community, of the Kyoto Protocol to the United Nations Framework Convention on Climate Change and the joint fulfilment of commitments thereunder. (Apr. 2002).

[14] EU Commission, European directive 2010/31/EU, of 19 may 2010, on energy efficiency on buildings (May 2010).

[15] EU Commission, European directive 2002/91/EU, of 16 december 2002, on energy efficiency on buildings (Dec. 2002).

[16] A. Henemann, BIPV: Built-in solar energy, Renewable Energy Focus 9 (6, Supplement) (2008) 14–19.

[17] M. Pagliaro, R. Ciriminna, G. Palmisano, BIPV: merging the photovoltaic with the construction industry, Progress in Photovoltaics: Research and Applications 18 (1) (2010) 61–72.

[18] T. Schuetze, Integration of photovoltaics in buildings—support policies addressing technical and formal aspects, Energies 6 (6) (2013) 2982–3001.

[19] A. Strzalka, N. Alam, E. Duminil, V. Coors, U. Eicker, Large scale integration of photovoltaics in cities, Applied Energy 93 (2012) 413–421.

[20] G. Quesada, D. Rousse, Y. Dutil, M. Badache, S. Hallé, A comprehensive review of solar facades. Opaque solar facades, Renewable and Sustainable Energy Reviews 16 (5) (2012) 2820–2832.

[21] IEA PVPS, Report IEA PVPS T1-30:2016. Trends 2016 in Photovoltaic Applications. Survey Report of Selected IEA Countries between 1992 and 2015, Tech. rep., IEA PVPS (2015).

27

Figure 12: Transposition models benchmark for all directions according to RMSD.

[22] S. M. Ivanova, Estimation of background diffuse irradiance on orthogonal surfaces under partially obstructed anisotropic sky. Part I – Vertical surfaces, Solar Energy 95 (2013) 376–391.

[23] N. Ouhajjou, W. Loibl, A. Anjomshoaa, S. Fenz, A. Tjoa, Ontology-based urban energy planning support: Building-integrated solar PV, 2015, pp. 543–550.

[24] Z. Sen, Solar energy in progress and future research trends, Progress in Energy and Combustion Science 30 (4) (2004) 367–416.

[25] World Meteorological Organization, Guide to the Global Observing System, Vol. 488, WMO, 2013.

[26] V. Badescu (Ed.), Modeling solar radiation at the Earth's surface, Springer Berlin Heidelberg, New York, 2008.

[27] M. Sengupta, A. Habte, S. Kurtz, A. Dobos, S. Wilbert, E. Lorenz, T. Stoffel, D. Renné, C. Gueymard, D. R. Myers, S. Wilcox, P. Blanc, R. Perez, Best practices handbook for the collection and use of solar resource data for solar energy applications (2015).

[28] WMO, Guide to Meteorological Instruments and Methods of Observation, 2010th Edition, Vol. 8 of WMO, WMO, 2010.

[29] M. de Simón-Martín, C. Alonso-Tristán, D. González-Peña, M. Díez-Mediavilla, New device for the simultaneous measurement of diffuse solar irradiance on several azimuth and tilting angles, Solar Energy 119 (2015) 370–382. doi:10.1016/j.solener.2015.06.001.

[30] J. L. Torres, M. de Blas, A. Garca, A. Gracia, A. de Francisco,

Sky luminance distribution in Pamplona (Spain) during the summer period, Journal of Atmospheric and Solar-Terrestrial Physics 72 (56) (2010) 382–388. doi:10.1016/j.jastp.2009.12.005.

[31] T. Muneer, W. E. Alnaser, F. Fairooz, The insolation on vertical surface having different directions in the Kingdom of Bahrain, Desalination 209 (13) (2007) 269–274. doi:10.1016/j.desal.2007.04.037.

[32] R. Perez, P. Ineichen, R. Seals, J. Michalsky, R. Stewart, Modeling daylight availability and irradiance components from direct and global irradiance, Solar Energy 44 (5) (1990) 271–289.

[33] Y. Q. Tian, R. J. Davies-Colley, P. Gong, B. W. Thorrold, Estimating solar radiation on slopes of arbitrary aspect, Agricultural and Forest Meteorology 109 (1) (2001) 67–74.

[34] E. Ruiz, A. Soler, L. Robledo, Comparison of the Olmo model with global irradiance measurements on vertical surfaces at Madrid, Energy 27 (10) (2002) 975–986. doi:10.1016/S0360-5442(02)00013-0.

[35] M. de Simón-Martín, M. Díez-Mediavilla, C. Alonso-Tristán, Shadow-band radiometer measurement of diffuse solar irradiance: Calculation of geometrical and total correction factors, Solar Energy 139 (2016) 85–99. doi:10.1016/j.solener.2016.09.026.

[36] B. A. LeBaron, J. J. Michalsky, R. Perez, A simple procedure for correcting shadowband data for all sky condi-

| | D01 | D02 | D03 | D04 | D05 | D06 | D07 | D08 | D09 | D10 | D11 | D12 | D13 | D14 | D15 | D16 | D17 | D18 | D19 | D20 | D21 | D22 | D23 | D24 | D25 | D26 | D27 | D28 | D29 | D30 |
|---|---|---|---|---|---|---|---|---|---|---|---|---|---|---|---|---|---|---|---|---|---|---|---|---|---|---|---|---|---|---|
| D30 | 17 | 17 | 17 | 6 | 16 | 26 | 25 | 7 | 4 | 15 | 8 | 23 | 13 | 18 | 3 | 11 | 24 | 21 | 5 | 12 | 10 | 9 | 14 | 19 | 22 | 20 | -1 | 1 | 2 | 0 |
| D29 | 15 | 15 | 15 | 4 | 14 | 24 | 23 | 5 | 2 | 13 | 6 | 21 | 11 | 16 | 1 | 9 | 22 | 19 | 3 | 10 | 8 | 7 | 12 | 17 | 20 | 18 | -3 | -1 | 0 | -2 |
| D28 | 16 | 16 | 16 | 5 | 15 | 25 | 24 | 6 | 3 | 14 | 7 | 22 | 12 | 17 | 2 | 10 | 23 | 20 | 4 | 11 | 9 | 8 | 13 | 18 | 21 | 19 | -2 | 0 | 1 | -1 |
| D27 | 18 | 18 | 18 | 7 | 17 | 27 | 26 | 8 | 5 | 16 | 9 | 24 | 14 | 19 | 4 | 12 | 25 | 22 | 6 | 13 | 11 | 10 | 15 | 20 | 23 | 21 | 0 | 2 | 3 | 1 |
| D26 | -3 | -3 | -3 | -14 | -4 | 6 | 5 | -13 | -16 | -5 | -12 | 3 | -7 | -2 | -17 | -9 | 4 | 1 | -15 | -8 | -10 | -11 | -6 | -1 | 2 | 0 | -21 | -19 | -18 | -20 |
| D25 | -5 | -5 | -5 | -16 | -6 | 4 | 3 | -15 | -18 | -7 | -14 | 1 | -9 | -4 | -19 | -11 | 2 | -1 | -17 | -10 | -12 | -13 | -8 | -3 | 0 | -2 | -23 | -21 | -20 | -22 |
| D24 | -2 | -2 | -2 | -13 | -3 | 7 | 6 | -12 | -15 | -4 | -11 | 4 | -6 | -1 | -16 | -8 | 5 | 2 | -14 | -7 | -9 | -10 | -5 | 0 | 3 | 1 | -20 | -18 | -17 | -19 |
| D23 | 3 | 3 | 3 | -8 | 2 | 12 | 11 | -7 | -10 | 1 | -6 | 9 | -1 | 4 | -11 | -3 | 10 | 7 | -9 | -2 | -4 | -5 | 0 | 5 | 8 | 6 | -15 | -13 | -12 | -14 |
| D22 | 8 | 8 | 8 | -3 | 7 | 17 | 16 | -2 | -5 | 6 | -1 | 14 | 4 | 9 | -6 | 2 | 15 | 12 | -4 | 3 | 1 | 0 | 5 | 10 | 13 | 11 | -10 | -8 | -7 | -9 |
| D21 | 7 | 7 | 7 | -4 | 6 | 16 | 15 | -3 | -5 | 5 | -2 | 13 | 3 | 8 | -7 | 1 | 14 | 11 | -5 | 2 | 0 | -1 | 4 | 9 | 12 | 10 | -11 | -9 | -8 | -10 |
| D20 | 5 | 5 | 5 | -6 | 4 | 14 | 13 | -5 | -3 | 3 | -4 | 11 | 1 | 6 | -9 | -1 | 12 | 9 | -7 | 0 | -2 | -3 | 2 | 7 | 10 | 8 | -13 | -11 | -10 | -12 |
| D19 | 12 | 12 | 12 | 1 | 11 | 21 | 20 | 2 | -1 | 10 | 3 | 18 | 8 | 13 | -2 | 6 | 19 | 16 | 0 | 7 | 5 | 4 | 9 | 14 | 17 | 15 | -6 | -4 | -3 | -5 |
| D18 | -4 | -4 | -4 | -15 | -5 | 5 | 4 | -14 | -17 | -6 | -13 | 2 | -8 | -3 | -18 | -10 | 3 | 0 | -16 | -9 | -11 | -12 | -7 | -2 | 1 | -1 | -22 | -20 | -19 | -21 |
| D17 | -7 | -7 | -7 | -18 | -8 | 2 | 1 | -17 | -20 | -9 | -16 | -1 | -11 | 6 | -21 | -13 | 0 | -3 | -19 | -12 | -14 | -15 | -10 | -5 | -2 | -4 | -25 | -23 | -22 | -24 |
| D16 | 6 | 6 | 6 | -5 | 5 | 15 | 14 | -4 | -7 | 4 | -3 | 12 | 2 | 7 | -8 | 0 | 13 | 10 | -6 | 1 | -1 | -2 | 3 | 8 | 11 | 9 | -12 | -10 | -9 | -11 |
| D15 | 14 | 14 | 14 | 3 | 13 | 23 | 22 | 4 | 1 | 12 | 5 | 20 | 10 | 15 | 0 | 8 | 21 | 18 | 2 | 9 | 7 | 6 | 11 | 16 | 19 | 17 | -4 | -2 | -1 | -3 |
| D14 | -1 | -1 | -1 | -12 | -2 | 8 | 7 | -11 | -14 | -3 | -10 | 5 | -5 | 0 | -15 | -7 | 6 | 3 | -13 | -6 | -8 | -9 | -4 | 1 | 4 | 2 | -19 | -17 | -16 | -18 |
| D13 | 4 | 4 | 4 | -7 | 3 | 13 | 12 | -6 | -9 | 2 | -5 | 10 | 0 | 5 | -10 | -2 | 11 | 8 | -8 | -1 | -3 | -4 | 1 | 6 | 9 | 7 | -14 | -12 | -11 | -13 |
| D12 | -6 | -6 | -6 | -17 | -7 | 3 | 2 | -16 | -19 | -8 | -15 | 0 | -10 | -5 | -20 | -12 | 1 | -2 | -18 | -11 | -13 | -14 | -9 | -4 | -1 | -3 | -24 | -22 | -21 | -23 |
| D11 | 9 | 9 | 9 | -2 | 8 | 18 | 17 | -1 | -4 | 7 | 0 | 15 | 5 | 10 | -5 | 3 | 16 | 13 | -3 | 4 | 2 | 1 | 6 | 11 | 14 | 12 | -9 | -7 | -6 | -8 |
| D10 | 2 | 2 | 2 | -9 | 1 | 11 | 10 | -8 | -11 | 0 | -7 | 8 | -2 | 3 | -12 | -4 | 9 | 6 | -10 | 3 | 5 | 6 | 1 | 4 | 7 | 5 | 16 | 14 | 13 | 15 |
| D09 | 13 | 13 | 13 | 2 | 12 | 22 | 21 | 3 | 0 | 11 | 4 | 19 | 9 | 14 | -1 | 7 | 20 | 17 | 1 | 8 | 6 | 5 | 10 | 15 | 18 | 16 | -5 | -3 | -2 | -4 |
| D08 | 10 | 10 | 10 | -1 | 9 | 19 | 18 | 0 | -3 | 8 | 1 | 16 | 6 | 11 | -4 | 4 | 17 | 14 | -2 | 5 | 3 | 2 | 7 | 12 | 15 | 13 | -8 | -6 | -5 | -7 |
| D07 | -8 | -8 | -8 | -19 | -9 | 1 | 0 | -18 | -21 | -10 | -17 | -2 | -12 | -7 | -22 | -14 | -1 | -4 | -20 | -13 | -15 | -16 | -11 | -6 | -3 | -5 | -26 | -24 | -23 | -25 |
| D06 | -9 | -9 | -9 | -20 | -10 | 0 | -1 | -19 | -22 | -11 | -18 | -3 | -13 | -8 | -23 | -15 | -2 | -5 | -21 | -14 | -16 | -17 | -12 | -7 | -4 | -6 | -27 | -25 | -24 | -26 |
| D05 | 1 | 1 | 1 | -10 | 0 | 10 | 9 | -9 | -12 | -1 | -8 | 7 | -3 | 2 | -13 | -5 | 8 | 5 | -11 | -4 | -6 | -7 | -2 | 3 | 6 | 4 | -17 | -15 | -14 | -16 |
| D04 | 11 | 11 | 11 | 0 | 10 | 20 | 19 | 1 | -2 | 9 | 2 | 17 | 7 | 12 | -3 | 5 | 18 | 15 | -1 | 6 | 4 | 3 | 8 | 13 | 16 | 14 | -7 | -5 | -4 | -6 |
| D03 | 0 | 0 | 0 | -11 | -1 | 9 | 8 | -10 | -13 | -2 | -9 | 6 | -4 | 1 | -14 | -6 | 7 | 4 | -12 | -5 | -7 | -8 | -3 | 2 | 5 | 3 | -18 | -16 | -15 | -17 |
| D02 | 0 | 0 | 0 | -11 | -1 | 9 | 8 | -10 | -13 | -2 | -9 | 6 | -4 | 1 | -14 | -6 | 7 | 4 | -12 | -5 | -7 | -8 | -3 | 2 | 5 | 3 | -18 | -16 | -15 | -17 |
| D01 | 0 | 0 | 0 | -11 | -1 | 9 | 8 | -10 | -13 | -2 | -9 | 6 | -4 | 1 | -14 | -6 | 7 | 4 | -12 | -5 | -7 | -8 | -3 | 2 | 5 | 3 | -18 | -16 | -15 | -17 |

Figure 13: Transposition models benchmark for all directions according to $\mu_{0.99}$.

tions, Solar Energy 44 (5) (1990) 249–256. doi:10.1016/0038-092X(90)90053-F.

[37] A. de Miguel, J. Bilbao, R. Aguiar, H. Kambezidis, E. Negro, Diffuse solar irradiation model evaluation in the North Mediterranean Belt area, Solar Energy 70 (2) (2001) 143–153. doi:10.1016/S0038-092X(00)00135-3.

[38] T. Muneer, Solar Radiation and Daylight Models, 2nd Edition, Vol. 1, ButterWorth-Heinemann, Oxford, 2004.

[39] G. López, T. Muneer, R. Claywell, Assessment of four shadow band correction models using beam normal irradiance data from the United Kingdom and Israel, Energy Conversion and Management 45 (13-14) (2004) 1963–1979. doi:10.1016/j.enconman.2003.11.001.

[40] Joint Committee for Guides in Metrology, Evaluation of measurement data: Guide to the expression of uncertainty in measurement. GUM 1995 with minor revisions, Bureau International des Poids et Mesures, 2008.

[41] C. A. Gueymard, A review of validation methodologies and statistical performance indicators for modeled solar radiation data: Towards a better bankability of solar projects, Renewable and Sustainable Energy Reviews 39 (2014) 1024–1034. doi:10.1016/j.rser.2014.07.117.

[42] R. J. Stone, Improved statistical procedure for the evaluation of solar radiation estimation models, Solar Energy 51 (4) (1993) 289–291.

[43] C. J. Willmott, Some comments on the evaluation of model performance, Bulletin of the American Meteorological Society 63 (11) (1982) 1309–1313. doi:10.1175/1520-0477(1982)063<1309:SCOTEO>2.0.CO;2.

[44] R. J. Stone, A nonparametric statistical procedure for ranking the overall performance of solar radiation models at multiple locations, Energy 19 (7) (1994) 765–769. doi:10.1016/0360-5442(94)90014-0.

[45] D. Moore, G. McCabe, Introduction to the Practice of Statistics, 3rd Edition, Vol. 1, W.H. Freeman and Company, New York, 2000.

[46] K. Taylor, Summarizing multiple aspects of model performance in a single diagram, Journal of Geophysical Research: Atmospheres 106 (D7) (2001) 7183–7192.

[47] D. Gough, J. Thomas, S. Oliver, Clarifying differences between review designs and methods, Systematic Reviews 1 (28) (2012) 1–9. doi:10.1186/2046-4053-1-28.

[48] E. Urra Medina, R. M. Barría Pailaquilén, La revisión sistemática y su relación con la práctica basada en la evidencia de la salud, Rev. Latino-Am 18 (4) (2010) 1–8.

[49] M. Meade, W. Richardson, Selecting and appraising studies for a systematic review, Annals of Internal Medicine 127 (7) (1997) 531–537.

[50] D. S. Broomhead, D. Lowe, Radial basis functions, multivariable functional interpolation and adaptive networks, Complex Systems 2 (1988) 21–355.

[51] J. Jang, ANFIS: Adaptative-network-based fuzzy inference

system, IEEE Transactions on Systems, Man and Cybernetics 23 (3) (1993) 665–685.

[52] B. Liu, R. Jordan, Daily insolation on surfaces tilted towards the equator, ASHRAE Journal 3 (1961) 53–59.

[53] V. Badescu, 3D isotropic approximation for solar diffuse irradiance on tilted surfaces, Renewable Energy 26 (2) (2002) 221–233.

[54] P. S. Koronakis, On the choice of the angle of tilt for south facing solar collectors in the Athens basin area, Solar Energy 36 (3) (1986) 217–225.

[55] F. J. Olmo, J. Vida, I. Foyo, Y. Castro-Diez, L. Alados-Arboledas, Prediction of global irradiance on inclined surfaces from horizontal global irradiance, Energy 24 (8) (1999) 689–704.

[56] E. G. Evseev, A. I. Kudish, An assessment of a revised Olmo et al. model to predict solar global radiation on a tilted surface at Beer Sheva, Israel, Renewable Energy 34 (1) (2009) 112–119.

[57] M. Lokmanhekim, Procedure for Determining Heating and Cooling Loads for Computerized Energy Calculations, ASHRAE, New York, 1971.

[58] M. Díez-Mediavilla, Medida y modelización de radiación solar difusa sobre plano inclinado, Ph.D. thesis, Universidad de Valladolid, Valladolid (2001).

[59] J. J. Hirsch, DOE-2: http://www.doe2.com. Last checked on May 2015 (2010).

[60] C. Gueymard, An anisotropic solar irradiance model for tilted surfaces and its comparison with selected engineering algorithms, Solar Energy 38 (5) (1987) 367–386.

[61] C. A. Gueymard, On the correct use of the Gueymard diffuse radiation model for tilted surfaces, Energy Conversion and Management 101 (2015) 787–788. doi:10.1016/j.enconman.2015.05.046.

[62] J. E. Hay, D. C. McKay, Calculation of solar irradiances for inclined surfaces: Verification of models which use hourly and daily data, in: IEA Task IX Final Report, Atmospheric Environment Service, Downsview, Canada, 1988.

[63] J. E. Hay, A revised method for determining the direct and diffuse components of the total short-wave radiation, Atmosphere 14 (4) (1976) 278–287.

[64] T. M. Klucher, Evaluation of models to predict insolation on tilted surfaces, Solar Energy 23 (2) (1979) 111–114.

[65] C. Ma, M. Iqbal, Statistical comparison of models for estimating solar radiation on inclined surfaces, Solar Energy 31 (3) (1983) 313–317.

[66] T. Muneer, Solar irradiance and illuminance models for Japan I: Sloped surfaces, Lighting Research and Technology 27 (4) (1995) 209–222.

[67] T. Muneer, Solar Radiation Modelling for the United Kingdom, Ph.D. thesis, Council for National Academic Awards, London (1987).

[68] R. Perez, R. Seals, P. Ineichen, R. Stewart, D. Menicucci, A new simplified version of the Perez diffuse irradiance model for tilted surfaces, Solar Energy 39 (3) (1987) 221–231.

[69] D. T. Reindl, W. A. Beckman, J. A. Duffie, Evaluation of hourly tilted surface radiation models, Solar Energy 45 (1) (1990) 9–17.

[70] J. A. Olseth, A. Skartveit, A probability density model for hourly total and beam irradiance on arbitrarily oriented planes, Solar Energy 39 (4) (1987) 343–351.

[71] A. Skartveit, J. Asle Olseth, Modelling slope irradiance at high latitudes, Solar Energy 36 (4) (1986) 333–344.

[72] M. Steven, H. Unsworth, The angular distribution and interception of diffuse solar radiation below overcast skies., Quarterly Journal Royal Meteorological Society 106 (447) (1980) 57–61.

[73] M. Steven, M. Unsworth, The diffuse solar irradiance of slopes

under cloudless skies (in Britain)., Quarterly Journal, Royal Meteorological Society 105 (445) (1979) 593–602.

[74] R. C. Temps, K. L. Coulson, Solar radiation incident upon slopes of different orientations, Solar Energy 19 (2) (1977) 179–184.

[75] C. J. Willmott, On the climatic optimization of the tilt and azimuth of flat-plate solar collectors, Solar Energy 28 (3) (1982) 205–216.

[76] A. P. Brunger, F. C. Hooper, Anisotropic sky radiance model based on narrow field of view measurements of shortwave radiance, Solar Energy 51 (1) (1993) 53–64.

[77] F. C. Hooper, A. P. Brunger, A model for the angular distribution of sky radiance, Journal of Solar Energy Engineering 102 (3) (1980) 196–202.

[78] N. Igawa, Y. Koga, T. Matsuzawa, H. Nakamura, Models of sky radiance distribution and sky luminance distribution, Solar Energy 77 (2) (2004) 137–157.

[79] N. Igawa, H. Nakamura, All sky model as a standard sky for the simulation of daylight environment, Building and Environment 36 (6) (2001) 763–770.

[80] P. Moon, D. E. Spencer, Illumination from a non-uniform sky, Vol. 37, New York, 1942.

[81] F. M. F. Siala, F. C. Hooper, A semi-empirical model for the directional distribution of the diffuse sky radiance, in: Renewables - a clean energy solution, Solar Energy Society of Canada, Otawa, 1989, pp. 322–326.

[82] M. T. Hagan, H. B. Demuth, M. H. Beale, O. de Jesús, Network Design, 2nd Edition, PWS Publishing, Boston, 1996.

[83] A. N. Celik, T. Muneer, Neural network based method for conversion of solar radiation data, Energy Conversion and Management 67 (2013) 117–124.

[84] T. Khatib, A. Mohamed, K. Sopian, A review of solar energy modeling techniques, Renewable and Sustainable Energy Reviews 16 (2012) 2864–2869. doi:10.1016/j.rser.2012.01.064.

[85] P. C. Jain, Modelling of the diffuse radiation in environment conscious architecture: The problem and its management, Solar & Wind Technology 6 (4) (1989) 493–500. doi:10.1016/0741-983X(89)90064-7.

[86] W. Yao, Z. Li, Q. Zhao, Y. Lu, R. Lu, A new anisotropic diffuse radiation model, Energy Conversion and Management 95 (2015) 304–313. doi:10.1016/j.enconman.2015.01.016.

[87] D. Yang, Solar radiation on inclined surfaces: Corrections and benchmarks, Solar Energy 136 (2016) 288–302.

[88] R. Wattan, S. Janjai, An investigation of the performance of 14 models for estimating hourly diffuse irradiation on inclined surfaces at tropical sites, Renewable Energy 93 (2016) 667–674. doi:10.1016/j.renene.2016.02.076.

[89] J. L. Threlkeld, Solar irradiation on surfaces on clear days, ASHRAE Journal 4 (1962) 43–54.

[90] D. G. Stephenson, Tables of solar altitude, azimuth, intensity and heat gain factors for latitudes from 43 to 55 degrees North, National Research Council of Canada. Division of Building Research, Otawa, 1967.

[91] K. Y. Kondratyev, Radiation in the Atmosphere, Academic Press, New York, 1969.

[92] T. Muneer, Solar radiation model for Europe, Building Services Engineering Research and Technology 11 (4) (1990) 153–163. doi:10.1177/014362449001100405.

[93] F. Kasten, A new table and approximation formula for the relative optical air mass, Architecture, Meteorology, Geophysics and Bioklimatology (1966) 206–223.

[94] K. J. A. Revfeim, A simple procedure for estimating global daily radiation on any surface, Journal of Applied Meteorology

17 (8) (1978) 1126–1131. doi:10.1175/1520-0450(1978)
017<1126:ASPFEG>2.0.CO;2.

[95] CIE, Spatial distribution of daylight - CIE standard general
sky (ISO 15469:2004 (E)/CIE S 011/E:2003) (2004).
URL http://www.cie.co.at/index.php/
Publications/index.php?i_ca_id=476

[96] M. A. Rosen, F. C. Hooper, A. P. Brunger, The characterization
and modelling of the diffuse radiance distribution under partly
cloudy skies, Solar Energy 43 (5) (1989) 281–290. doi:10.
1016/0038-092X(89)90115-1.

[97] D. Rumelhart, G. Hinton, R. Williams, Learning internal repre-
sentations by error propagation, MIT Press, Cambridge, 1986.

[98] W. McCulloch, W. Pitts, A logical calculus of the ideas im-
minent in neural nets, Bulletin of Mathematical Biophysics 5
(1943) 115–137.

[99] F. Rosenblatt, Principles of neurodynamics: Perceptrons and
the theory of brain mechanisms, Spartan, New York, 1962.

[100] Formulation of flow number of asphalt mixes using a hybrid
computational method, Construction and Building Materials
25 (3) (2011) 1338–1355. doi:10.1016/j.conbuildmat.
2010.09.010.

[101] W. M. Bolstad, Introduction to Bayesian Statistics, John Wiley,
New York, 2004.

[102] M. Gupta, R. Ragade, R. Yager, Advances in fuzzy set theory
and applications, North-Holland Pub. Co., New York, 1979.

[103] C. Gueymard, Direct and indirect uncertainties in the predic-
tion of tilted irradiance for solar engineering applications, So-
lar Energy 83 (3) (2009) 432–444.

[104] D. R. Myers, K. A. Emery, T. L. Stoffel, Uncertainty estimates
for global solar irradiance measurements used to evaluate PV
device performance, Solar Cells 27 (14) (1989) 455–464. doi:
10.1016/0379-6787(89)90055-0.

[105] D. R. Myers, Solar radiation modeling and measurements for
renewable energy applications: Data and model quality, in: In-
ternational Expert Conference on Mathematical Modeling of
Solar Radiation and Daylight - Challenges for the 21st Cen-
tury, Edinburgh, 2003, pp. 1–15.

[106] G. A. Kamali, I. Moradi, A. Khalili, Estimating solar radia-
tion on tilted surfaces with various orientations: A study case
in Karaj (Iran), Theoretical and Applied Climatology 84 (4)
(2006) 235–241.

[107] A. M. Noorian, I. Moradi, G. A. Kamali, Evaluation of 12
models to estimate hourly diffuse irradiation on inclined sur-
faces, Renewable Energy 33 (6) (2008) 1406–1412. doi:
10.1016/j.renene.2007.06.027.

[108] P. G. Loutzenhiser, H. Manz, C. Felsmann, P. A. Strachan,
T. Frank, G. M. Maxwell, Empirical validation of models to
compute solar irradiance on inclined surfaces for building en-
ergy simulation, Solar Energy 81 (2) (2007) 254–267.

[109] E. D. Mehleri, P. L. Zervas, H. Sarimveis, J. A. Palyvos,
N. C. Markatos, A new neural network model for evaluating
the performance of various hourly slope irradiation models:
Implementation for the region of Athens, Renewable Energy
35 (7) (2010) 1357–1362. doi:10.1016/j.renene.2009.
11.005.

[110] P. Yadav, S. Chandel, Comparative analysis of diffused solar
radiation models for optimum tilt angle determination for In-
dian locations, Applied Solar Energy (English translation of
Geliotekhnika) 50 (1) (2014) 53–59.